



HAL
open science

Oscillating grid turbulence in shear-thinning polymer solutions

T. Lacassagne, Serge Simoëns, M. El Hajem, A. Lyon, J.-Y. Champagne

► **To cite this version:**

T. Lacassagne, Serge Simoëns, M. El Hajem, A. Lyon, J.-Y. Champagne. Oscillating grid turbulence in shear-thinning polymer solutions. *Physics of Fluids*, 2019, 31 (8), pp.083102. 10.1063/1.5113551 . hal-02382786

HAL Id: hal-02382786

<https://hal.science/hal-02382786>

Submitted on 2 Nov 2021

HAL is a multi-disciplinary open access archive for the deposit and dissemination of scientific research documents, whether they are published or not. The documents may come from teaching and research institutions in France or abroad, or from public or private research centers.

L'archive ouverte pluridisciplinaire **HAL**, est destinée au dépôt et à la diffusion de documents scientifiques de niveau recherche, publiés ou non, émanant des établissements d'enseignement et de recherche français ou étrangers, des laboratoires publics ou privés.

1 Oscillating grid turbulence in shear-thinning polymer solutions

2 T. Lacassagne,^{1, a)} S. Simoëns,^{1, b)} M. EL Hajem,¹ A. Lyon,¹ and J.-Y. Champagne¹
3 *1 Univ Lyon, INSA de Lyon, Ecole Centrale de Lyon, Université Lyon 1, CNRS, LMFA UMR 5509, 69621 Villeurbanne Cedex,*
4 *France*

5 (Dated: July 18, 2019)

Oscillating grid apparatus are well known and convenient tools for the fundamental study of turbulence and its interaction with other phenomena, since they allow to generate turbulence supposedly homogeneous, isotropic, and free of mean shear. They could in particular be used to study turbulence and mass transfer near the interface between non-Newtonian liquids and a gas, as already done in air-water situations. Although frequently used in water and Newtonian fluids, oscillating grid turbulence generation has yet been rarely applied and never characterized in non-Newtonian media. The present work consists in a first experimental characterization of the flow properties of shear-thinning polymer (Xanthan Gum, XG) solutions stirred by an oscillating grid. Various polymer concentrations are tested for a single grid stirring condition. The dilute and semi-dilute entanglement concentration regimes are considered. Liquid phase velocities are measured by Particle Image Velocimetry (PIV). The existing mean flow that establishes in the tank is described and characterized, as well as turbulence properties (intensity, decay rate, length-scales, isotropy etc.). Oscillating grid turbulence (OGT) in dilute polymer solutions induces an enhanced mean flow compared to water, a similar decay behaviour with yet different decay rates, and enhanced turbulence large scales and anisotropy. In the semi-dilute regime of XG, turbulence and mean flows are essentially damped by viscosity. The evolution of mean flow and turbulence indicators leads to the definition of several polymer concentration sub-regimes, within the dilute one. Critical concentrations around 20 ppm and 50 ppm are found, comparable to drag reduction characteristic concentrations.

6 I. INTRODUCTION

7 Oscillating grid stirred tanks have been used for many
8 purposes in research on turbulence, for example the study
9 of interactions between turbulence and solid impermeable
10 boundaries^{1,2}, in stratified media³⁻⁶, or to study the behavior
11 of bubbles, cells, fibers and aggregates suspended in a turbu-
12 lent liquid phase⁷⁻¹⁰.

13 Such devices are said to generate quasi homogeneous and
14 isotropic turbulence in horizontal planes (parallel to the grid),
15 and to yield theoretically no mean flow, which is their ma-
16 jor advantage compared to fixed grid setups. The absence of
17 a strong mean shear avoids the destruction of complex flu-
18 ids' components (fibers, polymer chains, cells) that is some-
19 times observed in fixed grid turbulence¹¹. The fact that tur-
20 bulent structures are theoretically not advected by any mean
21 flow makes them more easily observable by advanced optical
22 techniques such as PIV and PLIF (Planar Laser Induced Flu-
23 orescence). It will yet be shown hereinafter that the validity
24 of this no-mean flow assumption is limited without any re-
25 duction of turbulent properties. Note that when a mean flow
26 does exist in oscillating grid systems, it takes the shape of a
27 set of stationary recirculation patterns, as will be extensively
28 discussed in this work. The term "mean flow" will hereinafter
29 refer to these recirculation, which can sometimes be called
30 "secondary recirculation" in the literature.

31 For the previous reasons, this type of device has been ex-
32 tensively used for the study of turbulence and gas-liquid mass
33 transfer at free surfaces¹²⁻¹⁵. The combination of numerical
34 simulations¹⁶⁻¹⁸ and experiments¹⁹⁻²³ has allowed to describe
35 the behavior of turbulence close to a flat air-water interface,

36 and the influence of this near surface turbulence on the fun-
37 damental and local mechanisms of gas dissolution into the
38 liquid phase. Yet these mechanisms are known to be mod-
39 ified when considering gas dissolution into a non-Newtonian
40 or surfactant-laden liquid phase. The influence of surface con-
41 tamination by surface active agents has already been the sub-
42 ject of numerical simulations^{24,25} and experimental works¹³,
43 but the effect of bulk fluid rheological properties remains to be
44 understood. This phenomenon is of great interest, since it is
45 frequently encountered in the chemical, pharmaceutical, and
46 process industries²⁶⁻²⁸. In this context, experiments of non-
47 Newtonian turbulence's interactions with flat free interfaces
48 are still needed. The convenience of oscillating grid setups,
49 often used in air-water situations, make them interesting can-
50 didates for such experiments.

51 Only a few studies of oscillating grid turbulence
52 (OGT) with non-Newtonian liquids can be found in the
53 literature²⁹⁻³¹, and none of them seems to tackle the effects
54 of variable viscosity on the possible mean flow and turbulence
55 properties mapping in the whole tank. Moreover, these studies
56 focus on turbulence below the grid, between the sweep region
57 and the bottom of the tank, for which the boundary condition
58 and thus mean flows are inherently different from the appli-
59 cation considered here. The aim of this paper is to study the
60 influence of a shear thinning behavior on the hydrodynamics
61 above the grid and below a free surface in an oscillating grid
62 stirred tank, as a first necessary step for a further investigation
63 of near surface turbulence and mass transfer in similar flu-
64 ids. Such properties are given to an initially Newtonian fluid,
65 water, by addition of a minute amount of polymer (Xanthan
66 Gum, XG). Fluid velocity measurements are achieved using
67 Particle Image Velocimetry (PIV) in a region of the tank lo-
68 cated between the upper position of the grid and the free sur-
69 face.

70 The objective is to describe precisely OGT in shear thin-
71 ning polymer solutions and see if its velocity field statistical

^{a)}Electronic mail: tom.lacassagne@gmail.com

^{b)}Electronic mail: serge.simoens@ec-lyon.fr

72 properties can be compared to OGT in water. In other words,
 73 can this device be used to generate controlled turbulence in
 74 such fluids, and does the hypothesis of a negligible mean flow
 75 remain valid? As an underlying question: can oscillating grid
 76 apparatus be used to study turbulence near a free surface in
 77 shear thinning polymer solutions? To do so, indicators of tur-
 78 bulence and mean flow topology are extracted. The effects of
 79 polymer concentration on the existing mean flow topology are
 80 first studied. The evolution of turbulence properties with the
 81 distance from the grid and polymer concentration is then ad-
 82 dressed. Finally, possible causes for the apparent mean flow
 83 enhancement are discussed, and the different concentration
 84 regimes evidenced are compared to drag reduction character-
 85 istics of XG.

86 II. BACKGROUND

87 A. Oscillating grid turbulence in Newtonian liquids

88 The principle of an Oscillating Grid apparatus is to pro-
 89 duce turbulence by making a grid oscillate at a frequency f
 90 and with an amplitude or stroke S . It is commonly said that
 91 the jets and wakes behind the grid's holes and bars interact
 92 to generate turbulence^{3,4,14,32}, which then diffuses away from
 93 the grid. Turbulence can be studied either above⁴ or below
 94 the grid⁶, the bottom boundary condition being a rigid wall,
 95 and the top boundary condition either a rigid wall³ or a free
 96 surface²⁰. The first oscillating grid apparatus were designed
 97 by Rouse and Dodu³³ and Bouvard and Dumas³⁴, but full
 98 characterization of OGT in prismatic tanks only came with
 99 the pioneer works of Thompson and Turner³ and Hopfinger
 100 and Toly⁴ (that are respectively referred to as TT and HT later
 101 in the manuscript).

102 1. Turbulence properties

103 When fulfilling a set of conditions on grid shape, solidity
 104 and distance from the bottom of the tank defined by the previ-
 105 ous authors, OGT is supposed to yield a quasi-homogeneous
 106 and isotropic turbulence with negligible mean flow. Homo-
 107 geneity and isotropy are achieved in horizontal planes, far
 108 enough from the walls and from the grid's extreme positions
 109 (2 or 3 times the mesh size M defined below, depending on the
 110 study).

111 Expressions for the root mean square (rms) of horizontal
 112 and vertical velocity fluctuations, respectively denoted u'_x and
 113 u'_z , as a function of the distance from the grid z have been
 114 derived respectively by Hopfinger and Toly⁴ as:

$$\begin{aligned} u'_x &= C_{1HT} \cdot f \cdot S^{1.5} \cdot M^{0.5} \cdot z^n \\ u'_z &= C_{2HT} \cdot u'_x \end{aligned} \quad (1)$$

115 Where f is the grid frequency, S the amplitude of oscilla-
 116 tions (or Stroke), and the mesh size M . An expression for the
 117 evolution of the horizontal integral length scale of turbulence
 118 L with z comes from the work of Thompson and Turner³:

$$L = C_{TT} \cdot z \quad (2)$$

119 Where, $C_{TT} \simeq 0.1$, $C_{1HT} \simeq 0.25$, $C_{2HT} \simeq 1.2$, and $n = -1$
 120 in the original works. These relationships have been verified
 121 by a number of studies^{5,6,12,14,35-39}. The values of the differ-
 122 ent constants vary among the works in the following ranges:
 123 $C_{TT} \in [0.1..0.4]$, $C_{1HT} \in [0.2..0.3]$, $C_{2HT} \in [1.1..1.4]$. The
 124 proportionality coefficient between the integral length scale
 125 and the distance to the grid C_{TT} was also found to depend on
 126 the S/M ratio^{4,40}.

127 It should also be noted that the previous laws are valid for
 128 turbulence both above and below the grid^{4,6}, regardless of the
 129 boundary condition, except at the vicinity of the either liq-
 130 uid/solid or liquid/gas interface where turbulence is affected
 131 by boundary layer interactions^{1,2,12,23}. However, mean flow
 132 patterns that develop in the tank should depend on boundary
 133 conditions. In this work, we will more specifically focus on
 134 the case of the flow above the grid and below a free surface.

135 2. Mean flow

136 At first, the concept of OGT generating no mean flow,
 137 but only isotropic and homogeneous turbulence, was rather
 138 well believed. With the development of PIV techniques al-
 139 lowing further spatial investigations of the flow inside OGT
 140 tanks, it became clear that a mean flow always establishes,
 141 even when matching the previous requirements. McKenna
 142 and McGillis⁴¹ showed the existence of persistent mean flow
 143 structures, with relative high kinetic energy level as compared
 144 to the turbulent kinetic energy. Moreover, this mean flow
 145 seems to be poorly repeatable and strongly dependent on ini-
 146 tial conditions¹⁴. It is therefore really hard to predict the mean
 147 flow that could occur in the oscillating tank during a spe-
 148 cific measurement, and this is one of the main limitations of
 149 OGT systems. Oscillating grid apparatus should thus be seen
 150 as ways of generating controlled turbulence with low mean
 151 flow rather than as a tool to produce completely mean shear
 152 free, homogeneous and isotropic turbulence. McCorquodale
 153 and Munro⁴² recently suggested a method for reducing mean
 154 flows in OGT using an inner box placed inside the stirred tank
 155 to separate the wall-induced vortices from the rest of the flow.
 156 This will be discussed in section V B.

157 Nevertheless, it is important to point out that all the previ-
 158 ous conclusions are yet only valid and established when con-
 159 sidering OGT in water (or other Newtonian fluids). Character-
 160 ization of turbulence velocity fluctuations and integral length
 161 scales, and evidence of mean flows associated to OGT in shear
 162 thinning polymer solutions are yet to be performed. This is the
 163 scope of this study. In order to understand the changes that
 164 may arise upon polymer addition, the following paragraphs
 165 briefly summarize the literature of turbulence in polymer solu-
 166 tions. Studies involving grid turbulence in polymer solutions
 167 are detailed in section II C.

168 B. Drag reduction and turbulence in polymer solutions

169 It has been known since the late 1940's⁴³ that a very small
170 concentration of polymer diluted in a solvent could drastically
171 reduce drag. This phenomenon is called drag reduction, since
172 it may decrease the pressure drop in a pipe by up to 80 %⁴⁴.
173 As it is of paramount interest in many applications such as
174 hydraulics systems or oil and gas industry, a huge number of
175 studies have already addressed this topic⁴⁵.

176 Since OGT is driven both by large scale motion of the grid
177 and by boundary layer interactions at the grid's bar level, drag
178 reduction should be one of the mechanisms at the origin of
179 the modification of flow properties by the polymer. The basic
180 principle is that the polymer molecules introduced in the
181 solvent act as molecular springs, undergoing coil-stretch tran-
182 sition thus storing part of the kinetic energy of the flow^{46,47}.
183 This is especially efficient in high shear regions close to the
184 walls and leads to an apparent increase in the buffer layer
185 thickness of the boundary layer and a drastic reduction of the
186 friction. For a given concentration of polymer, the friction
187 coefficient variations as a function of the Reynolds number
188 departs from the classical Prandtl-Karman law when reaching
189 an onset Reynolds number. This is called the onset of drag
190 reduction⁴⁷. The higher the polymer concentration, the lower
191 the Reynolds number at the onset. When further increasing Re
192 after the onset, the friction factor decreases extremely rapidly
193 until it reaches an asymptotic trend. Depending on the nature
194 of the polymer, two types of drag reduction leading to two
195 asymptotic slopes are possible. In type A drag reduction, the
196 friction coefficient tends to what is called the maximum drag
197 reduction asymptote empirically determined by Virk⁴⁸ (see
198 Sreenivasan and White⁴⁷, figure 1). In type B drag reduction,
199 it ultimately follows a Prandtl-Karman slope shifted towards
200 lower friction coefficients⁴⁹. The drag reduction level of this
201 last curve is fixed by the polymer concentration. Type A is
202 characteristic of flexible random coiled and highly deformable
203 polymer chains (eg. PolyEthylene Oxide, PEO), and type B of
204 relatively rigid, elongated and undeformable molecules. XG
205 studied here is of this second type⁵⁰. This last observation
206 stresses the importance of polymer conformation and rigidity
207 in its interactions with the flow.

208 The physical mechanisms of drag reduction relies on the in-
209 teractions between polymer chains and the flow, and the scales
210 at which polymers can take or give energy to the fluid. Poly-
211 mer chains' structure gives them the ability to deform elasti-
212 cally and store energy at small scales⁴⁶, which tends to trun-
213 cate or modify the flow energy cascade before reaching the
214 Kolmogorov scale⁵¹⁻⁵⁵. Such interactions should also impact
215 turbulence in the homogeneous isotropic case, without high
216 shear and boundary layers effects. It has been shown from
217 direct numerical simulations^{56,57} and experiments^{53,58-60} that
218 the Eulerian quantities of the bulk turbulence (strain, enstro-
219 phy, Reynolds stress, velocity gradients fields) are strongly re-
220 duced at small scales in viscoelastic solutions. The same con-
221 clusions can also be drawn using an experimental Lagrangian
222 approach. Crawford *et al.*⁶¹ for example performed time re-
223 solved measurement of Lagrangian acceleration of tracer par-
224 ticles in a *washing-machine* turbulence and found that the

225 rms and isotropy of particle accelerations were substantially
226 decreased in dilute polymer solutions as compared to water.
227 Viscous dissipation is reduced as the dissipation by the poly-
228 mer chain increases: polymer chains store energy at small
229 scales and so the small scales of turbulence are damped. But
230 the effect of polymer also propagates to larger scales. This
231 can translate for example into an increase of integral length
232 scales and of large scale fluctuations of velocity^{56,59,60}. This
233 is also the case in inelastic shear-thinning solutions⁶². Nguyen
234 *et al.*⁵⁵ recently studied the flow-polymer interactions in the
235 dissipative range and showed that the polymer pumps energy
236 at small scale when it is deformed by flow structures, and
237 can give back a part of this energy to the flow when relax-
238 ing, thus explaining the up-scales propagation observed ex-
239 perimentally. As for OGT, we should thus expect an influence
240 of the polymer on the large scale flow patterns. This is indeed
241 described in section IV A.

242 In channels or pipes, most of the strain field to be re-
243 duced can be found near the walls, and the forcing is done
244 at small scales (roughness of the wall), hence the polymer
245 effects are felt at low concentrations, typical of drag reduc-
246 tion. For example, Cai *et al.*⁶³ observed that viscoelastic-
247 ity strongly decreased both the frequency and the intensity of
248 burst events generated at the bottom of a channel flow by in-
249 hibiting the small scale coherent structures in the sheared sub-
250 layer. However, when forcing turbulence by energy injection
251 at scales larger than the cutoff scale, polymers do not play
252 a role at the turbulence production step, and non-Newtonian
253 effects are found to appear for concentrations larger than typ-
254 ical drag reduction concentrations⁵⁹. Finally, an interesting
255 feature observed in flows with strong mean shears such as
256 channel flows^{63,64} is an increase of turbulence anisotropy. It
257 comes from the tendency of polymer chains to align with the
258 main shear direction, leading to an increase in tangential ve-
259 locity fluctuations and a decrease in the normal ones. This
260 effect was lately observed to happen during the propagation
261 of a turbulent/non-turbulent interface as well, where polymer
262 chains tend to align with the turbulent front⁵⁷. Apart from
263 elasticity, shear-thinning induced by the presence of polymer
264 chains is also known to affect many features of flows, turbu-
265 lent or not, from large to small scales, as described recently in
266 several works^{62,65,66}.

267 C. Grid turbulence in polymer solution

268 The influence of non-Newtonian behavior on grid
269 turbulence has been mainly studied for fixed grid
270 configuration^{44,67-71}. It was found that grid turbulence
271 for such fluids was much more anisotropic, as expected from
272 flows with a preferential shear direction, but also that it de-
273 cayed more slowly. Recently, Vonlanthen and Monkewitz¹¹
274 used PIV measurements to look at turbulent spectra and scales
275 in grid turbulence of dilute polymer solutions and evidence
276 high Reynolds number viscoelastic turbulence. In their
277 experiments, they found that both the shape of the energy
278 spectrum and the elastic ("Lumley") scale evolved with time,
279 which they explained by the destruction of polymer chains by

280 the strong shears in the vicinity of the grid. This shows one of
 281 the limits of fixed grid devices for the study of turbulence in
 282 polymer solutions: reaching high levels of turbulence requires
 283 high flow rates which may cause important degradation of the
 284 polymer throughout the measurements. One may thus prefer
 285 using OGT rather than fixed grid.

286 Citing Vonlanthen and Monkewitz¹¹, "*The difference be-*
 287 *tween the effect of polymers on turbulence without and with*
 288 *mean shear is that in the former case the polymers can only*
 289 *provoke additional local energy dissipation, while in the lat-*
 290 *ter case they can in addition modify the mean shear and with*
 291 *it long-range energy exchange by instabilities". The non-*
 292 *Newtonian properties of the fluid are in such a way supposed*
 293 *to affect the OGT turbulence decay law, since they act on lo-*
 294 *cal turbulence dissipation. The previous sentence also implies*
 295 *that the secondary flows inside the grid stirred tank are very*
 296 *likely to be different in dilute polymer solution than for the*
 297 *Newtonian case.*

298 The first study of OGT in viscoelastic dilute polymer so-
 299 lutions (PEO) was made by Liberzon *et al.*²⁹, who observed
 300 the velocity propagation of the boundary between turbulent
 301 and non-turbulent regions in the tank, at the first instants after
 302 the onset of the grid's oscillations. They found that the tur-
 303 bulent/non turbulent interface moved globally faster in dilute
 304 polymer solution than in water. However, the characteristics
 305 of turbulence and mean flow in a steady state are not men-
 306 tioned, and the author later admitted that results could have
 307 been contaminated by the presence of mean shear at the walls
 308 of the tank (*i.e.* by the unexpected mean flow)⁵⁷.

309 Wang *et al.*^{30,31} later used a two oscillating grid device to
 310 study the viscoelastic effects of surfactants and dilute poly-
 311 mer on coherent structures. They confirmed that the addition
 312 of polymer tends to decrease the small scale effects of tur-
 313 bulence, and that this decrease can not only be attributed to
 314 the overall viscosity increase, since it is not associated with a
 315 decrease of the turbulent kinetic energy. The non-Newtonian
 316 property of the flow seemed to strongly modify the spectrum
 317 of turbulent structures at large wave numbers. They also
 318 found that the turbulent small scale suppression effect arose
 319 only when reaching a critical polymer concentration (unfor-
 320 tunately not quantified), which may not be the same in OGT
 321 than in channel flows or fixed grid experiments, and seems
 322 to be higher than the critical concentration for drag reduction
 323 effects.

324 To our best knowledge, no existing study mentions the pos-
 325 sible mean flow that could have developed in grid stirred
 326 tanks, and even less its probable polymer concentration de-
 327 pendency. Moreover, the previous studies focused on the case
 328 of a viscoelastic polymer solution while the fluid studied here
 329 is shear thinning and inelastic. The evolution of stationary
 330 turbulence properties with the distance from the grid, such as
 331 turbulent kinetic energy and velocity fluctuations rms also re-
 332 main unknown in single oscillating grid systems with dilute
 333 polymer solutions (e.g., can profiles analog to HT's law 1 be
 334 exhibited?). The aim of this work is thus to characterize both
 335 these turbulence properties and the mean flow that possibly
 336 establishes in the tank.

C_{XG} (ppm)	μ_0 (mPa s)	μ_∞ (mPa s)	t_{CY} (s)	a	p
10	1.30×10^0	0.99	0.08	2.00	0.60
25	3.97×10^0	0.95	0.45	2.00	0.57
50	1.09×10^1	1.09	0.55	2.00	0.50
100	3.28×10^1	1.05	1.60	2.00	0.50
500	2.03×10^2	1.05	2.23	1.27	0.45
1000	4.43×10^3	1.13	2.23	0.93	0.38
2000	1.94×10^3	2.73	3.15	0.72	0.25
10000	5.50×10^4	3.73	75.44	2.00	0.28

Table I. Carreau-Yasuda fitting parameters for the shear thinning behavior of XG solutions at various concentrations.

337 III. MATERIALS AND METHODS

338 A. Polymer solutions

339 Shear-thinning properties are conferred to the liquid by ad-
 340 dition of Xanthan Gum (XG), into distilled water. Here XG
 341 produced by Kelco under the commercial name Keltrol CG-T
 342 is used. Its average molar mass is $M_w = 3.4 \times 10^6$ g mol⁻¹ and
 343 its polydispersity equal to 1.12⁷². XG is chosen for its high
 344 resistance to strong shear and extreme temperature and pH
 345 conditions⁷³. Such features are useful when using it nearby a
 346 rigid oscillating grid (which can locally crate high shears), and
 347 for future studies of scalar transfer at gas-liquid interfaces⁷⁴.
 348 The rheological properties of such solutions have been mea-
 349 sured using a MCR 302 Anton Paar Rheometer. Their shear
 350 thinning behavior is modeled by a Carreau-Yasuda (CY) equa-
 351 tion :

$$\frac{\mu - \mu_\infty}{\mu_0 - \mu_\infty} = (1 + (t_{CY}\dot{\gamma})^a)^{\frac{p-1}{a}} \quad (3)$$

352 Where the zero shear rate and infinite shear rate Newtonian
 353 viscosities (resp. μ_0 and μ_∞), characteristic time scale t_{CY} ,
 354 and exponents a and p depend on the polymer concentration
 355 C_{XG} . The power law decay exponent of viscosity with the
 356 increasing shear rate is (p-1). a is a parameter for the transition
 357 between power law and Newtonian behaviours. Their values
 358 are reported in table I for C_{XG} variations over 3 decades.

359 By plotting the evolution of the characteristic timescale
 360 with polymer concentration (figure 1), one can clearly evi-
 361 dence the three main entanglement concentration domains for
 362 XG in aqueous salt-free solutions defined by Cuvelier and
 363 Launay⁷⁵ and Wyatt and Liberatore⁷⁶.

- 364 • The dilute regime (D) in which the interaction between
 365 isolated polymer chains and the flow are dominant, and
 366 interactions of polymer chains between each other are
 367 negligible.
- 368 • The semi-dilute (SD) regime, in which the electro-
 369 static and mechanical interactions between molecule
 370 becomes significant
- 371 • The concentrated (C) regime, for which chain entan-
 372 glement is the dominant mechanism of the liquid phase
 373 rheology.

374 The transition concentration between the three regimes are
 375 identical to the ones observed by Wyatt and Liberatore⁷⁶, and
 376 so are the zero shear rate viscosity magnitudes. Time scales
 377 measured for the present study are typically one order of mag-
 378 nitude lower. This is explainable by the fact that the proper-
 379 ties of XG are very sensitive to the molar mass M_w of the
 380 polymer, which depends itself on production and dissolution
 381 conditions⁷³. Moreover, in order to avoid the formation of
 382 disordered chains during dissolution, and ensure the repro-
 383 ductibility of measurements, special care has to be taken in
 384 the process of dissolving XG. Only distilled water is used wi-
 385 thout adding any salt, and moderate stirring and heating con-
 386 ditions are applied as specified by Garcia-Ochoa *et al.*⁷³. In
 387 this rheological characterization, the uncertainty on C_{XG} is of
 388 the order of 1%. The procedure used for the fabrication of XG
 389 solutions for PIV experiments yields uncertainty up to 10% on
 390 C_{XG} (see Lacassagne⁷⁴ appendix A). The associated horizon-
 391 tal error bars are not shown on following figures in the interest
 392 of clarity, but this uncertainty has to be kept in mind, espe-
 393 cially when discussing critical polymer concentrations in sec-
 394 tion V A. In this work, the concentration range between 0 and
 395 500 ppm is explored. The focus is made on the dilute regime.
 396 The onset of the semi-dilute regime is also considered, but
 397 no measurement is performed in the inner semi-dilute regime
 398 evidenced by Wyatt and Liberatore⁷⁶ between 100 ppm and
 399 200 ppm (see figure 1 a), slope equal to -0.5).

400 B. Oscillating grid setup

401 Turbulence is generated in a transparent tank of a 277 mm
 402 by 277 mm inner cross section. The fluid height is set at
 403 $H_f = 450$ mm and the distance between the surface and the
 404 average grid position is 250 mm. The vertical axis, oriented
 405 upwards, is noted z , and x and y are the axis defined by the
 406 grid bars. The origin of the reference frame is placed at the
 407 grid average position ($z=0$) at the crossing between the two
 408 central bars. In this study only polymer concentration is var-
 409 ied and all oscillations parameters are kept constant. The grid
 410 has square section bars of width equal to 7 mm, and the mesh
 411 parameter (distance between two grid bars) is $M = 35$ mm.
 412 This yields a solidity of 0.36, below the maximum value of
 413 0.4 recommended by Thompson and Turner³. The frequency
 414 is fixed at $f = 1$ Hz and the Stroke at $S = 45$ mm. It allows to
 415 define a grid-based Reynolds number using the definition of
 416 Janzen *et al.*²⁰, using the zero shear rate viscosity:

$$417 \quad Re_g = \frac{\rho f S^2}{\mu_0} \quad (4)$$

418 The density ρ of the fluid is assumed equal to that of wa-
 419 ter, because of the very small mass of polymer added. For
 420 this range of grid Reynolds number, it has been checked that
 421 polymer chains are indeed not destroyed during the experi-
 422 ments (maximum 2 hours of duration) by comparing viscosity
 423 curves of the solution before and after the experiment. Finally,
 424 in order to quantify the ratio between the polymer relaxation

425 time scale and the grid forcing time scale, the grid based Deb-
 426 orah number De is defined as:

$$427 \quad De = \frac{t_{CY}}{T} = t_{CY} f \quad (5)$$

428 with T the period of oscillations. Values of Re_g and De are
 429 reported in table II for each concentration studied.

428 C. PIV Measurements

429 Liquid phase velocity measurements in the tank are
 430 achieved by Particle Image Velocimetry (PIV). The experi-
 431 mental setup is sketched in figure 2. The region of interest
 432 (ROI) is a vertical rectangle, in plane (\vec{x}, \vec{z}) . Its width is close
 433 to that of the tank, and it includes fluid heights between the
 434 grid's top position and the free surface. The cameras used
 435 are double frame LaVision sCmos sensors of 2560 by 2160
 436 pixels, equipped with a 50 mm focal Macro lens. A pulsed
 437 Quantel Nd:YAG laser emitting at $\lambda = 532$ nm is used to il-
 438 luminate 50 μm diameter polyamide particles. The colimated
 439 laser sheet thickness achieved is 200 μm . It is estimated by
 440 marking a photosensitive paper band placed on the wall of the
 441 tank closer to the laser head with a single laser pulse.

442 Depending on polymer concentration, the order of magni-
 443 tude of measured velocities may differ considerably. In or-
 444 der to keep the measured particle displacement of the order of
 445 one third of the interrogation window, two types of PIV are
 446 used: double frame PIV for $C_{XG} < 250$ ppm, and single frame
 447 PIV for $C_{XG} \geq 250$ ppm. In the first case, the acquisition fre-
 448 quency f_{acq} is 4 Hz, and the time interval between laser pulses
 449 is $\Delta t = 18$ ms. In the second case, $f_{acq} = 10$ Hz and consequently
 450 $\Delta t = 100$ ms. Vector fields are computed with DaVis 8 software
 451 using a multipass processing: a first pass with 64 by 64 pixels
 452 and 2 following passes with 32 by 32 pixels round Gaussian
 453 weighted interrogation windows, at a maximum 50% overlap.
 454 Spurious vectors are removed from PIV fields by applying a
 455 threshold of 1.2 on the peak ratio, and replaced using median
 456 filtering (always less than 10% of the total number of vectors).

457 The final spatial resolution achieved is 2.3 mm. The small-
 458 est Kolmogorov length scale and Taylor micro scales of tur-
 459 bulence are supposed to be found in the water case, for which
 460 the viscosity is always the lowest. Based on the velocity and
 461 length scales order of magnitudes shown in figures 7 and 9
 462 (scales arbitrarily taken at $z=20$ mm), Kolmogorov and Tay-
 463 lor length scales are evaluated to be respectively of about
 464 0.19 mm and 2.24 mm. For 100 ppm XG solutions, using a
 465 constant viscosity equal to μ_∞ , they increase to 0.33 mm and
 466 3.25 mm, and up to 4.35 mm and 18.17 mm when using μ_0
 467 as the scale viscosity. The 2.3 mm spatial resolution is thus
 468 quite coarse and would unfortunately not allow to evidence
 469 energy variations at large wave numbers characteristic of high
 470 Reynolds number viscoelastic turbulence. It is yet sufficient
 471 to discuss the and large scale effects.

472 1000 vector fields are recorded for each run, correspond-
 473 ing to a measurement time of 250 s at $f_{acq} = 4$ Hz and 100 s
 474 at $f_{acq} = 10$ Hz. Assuming the integral time-scale of turbu-
 475 lence to be of the order of magnitude of the grid period (this

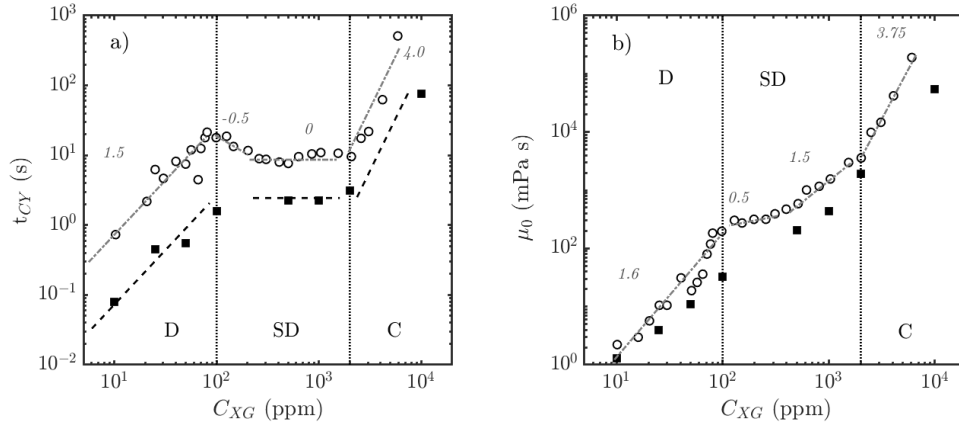


Figure 1. Evolution of characteristic time scale t_{CY} (a) and zero shear rate viscosity μ_0 (b) with polymer concentration C_{XG} . Data and trends for the present study (resp. full squares and dashed lines) are compared to the work of Wyatt and Liberatore⁷⁶ (empty circles and dashed-dotted lines, for which the slopes are indicated by italic numbers). Dilute (D), semi-dilute (SD) and concentrated (C) concentration regimes are separated by dotted lines at $C_{XG} = 100$ ppm and $C_{XG} = 2000$ ppm on both sub-figures.

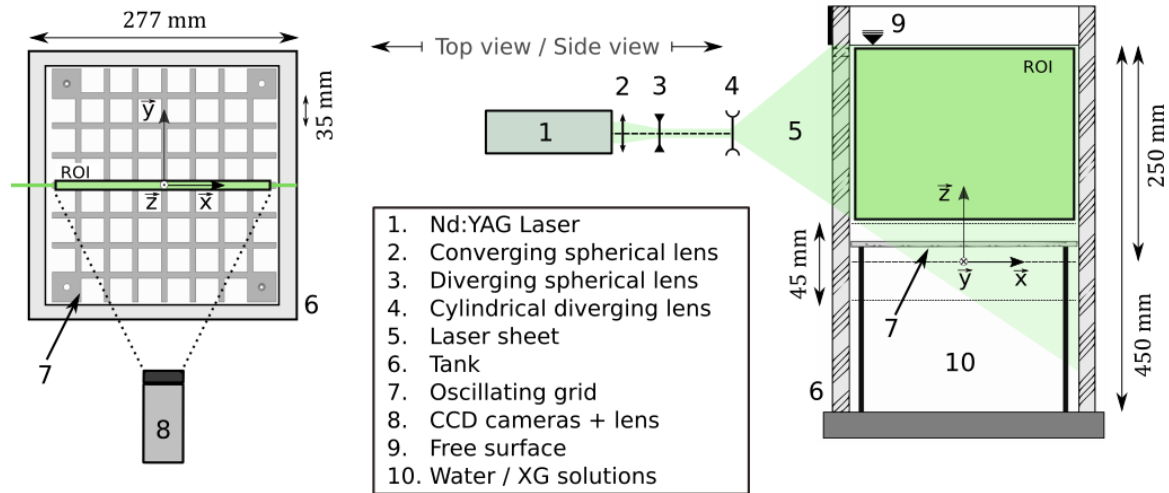


Figure 2. Sketch of the oscillating grid and PIV setup.

476 hypothesis could be checked for water and dilute regime XG
 477 solutions), this ensures a statistical analysis over at least 100
 478 uncorrelated events. Each experiment is moreover performed
 479 twice.

480 In order to check for statistical convergence and estimate
 481 uncertainty on velocities, sliding statistics on 500 subsequent
 482 snapshots (time interval equal to $1/f_{acq}$) are computed for
 483 both experiments. For mean velocities, and rms of velocity
 484 fluctuations, uncertainties are then estimated as the standard
 485 deviation of the variations of these samples' statistics around
 486 the "statistically converged" result obtained using the full data
 487 range. Typical velocity uncertainties thus evaluated are $\pm 6\%$
 488 and $\pm 5\%$ for respectively mean and rms quantities (spatial av-
 489 erage on the whole ROI). Statistical convergence is ensured up
 490 to the previous confidence intervals.

491 IV. RESULTS

492 A. Mean flows and re-circulations

493 1. Topology of the mean flow

494 The existence of mean flows and recirculations is most of
 495 the time an unwanted feature of OGT, which was initially
 496 meant to study turbulence alone in absence of mean shear⁴,
 497 but can unfortunately not be avoided. They are supposedly
 498 due to the grid tendency to drift out of alignment, and to initial
 499 minor fluid motion favouring the development of large
 500 scale motion and allowing mean flow patterns to persist once
 501 developed⁷⁷. In the ROI, the mean flow is structured in two
 502 main recirculation vortices close to the grid and near the walls.
 503 Figure 3 shows in three columns respectively the average ve-

504 locity field magnitude $\sqrt{\overline{U}_x^2 + \overline{U}_z^2}$ (with \overline{U}_x and \overline{U}_z respec- 557
 505 tively the horizontal and vertical mean flow components), the 558
 506 associated streamlines, and the vorticity of the average veloc- 559
 507 ity field $\overline{\Omega} = \nabla \wedge \overline{\mathbf{U}}$. These quantities are represented for wa- 560
 508 ter (first line) and three polymer concentrations: one in the 561
 509 dilute regime (10 ppm, second line), one in the semi-dilute 562
 510 regime (500 ppm last line) and one in the transition region 563
 511 (100 ppm, third line). The recirculation patterns observed on 564
 512 the streamline figures (central column) are evidenced by two 565
 513 opposite sign high magnitude vorticity patches on both sides 566
 514 of the tank, just above the grid sweep zone (right column). 567
 515 Isovalue lines of vorticity are drawn at the arbitrary threshold 568
 516 $\overline{\Omega} = \pm 0.02 \overline{\Omega}_m$ which $\overline{\Omega}_m$ the maximum vorticity value at a 569
 517 given concentration defined section IV A 2. They represent 570
 518 an arbitrary estimation of the boundaries of the mean flow 571
 519 vortices. Similar flow patterns have also been observed by 572
 520 McKenna and McGillis¹³ for water.

521 Based on the observation of figure 3 and additional inter- 573
 522 mediate concentrations (18, 25, 35, 50, 75, 150 and 250 ppm, 574
 523 not shown in the figure), the effect of polymer addition on 575
 524 the mean flow seems to be the following. When adding poly- 576
 525 mer to water, the flow organizes into two main regions dom- 577
 526 inated by the two counter rotative side vortices illustrated by 578
 527 the streamlines or the vorticity isovalues. Increasing polymer 579
 528 concentration first causes the mean flow vortices to grow in 580
 529 size until they reach the top of the fluid volume, at a concen- 581
 530 tration between 10 and 25 ppm. The flow is then divided into 582
 531 two main regions separated by a global up-going region at 583
 532 the center of the plane for concentrations between 25 and 100 584
 533 ppm, as seen on figures 3, left and central columns. A further 585
 534 increase in concentration leads to the collapse of these recir- 586
 535 culating regions: their size reduces (figure 3 central and right 587
 536 columns), and the central up-flowing region progressively dis- 588
 537 appears. Hypothesis will later be made on the probable rea- 589
 538 sons for this higher concentration behavior.

539 2. Mean flow indicators

540 Simple indicators can be defined in order to measure the in- 595
 541 tensity and region of influence of the mean flow, and quantify 596
 542 the mean flow enhancement.

- 543 • The first criterion is the value of the curl of the average 599
 544 velocity field at the center of the side vortices. This is 600
 545 a measurement of the maximum vorticity in the mean 601
 546 flow, and thus of the intensity of the side eddies. Here 602
 547 it is defined as $\overline{\Omega}_m = \max(\overline{\Omega}(O_A), \overline{\Omega}(O_B))$ where O_A is 603
 548 the central point of the left vortex and O_B the central 604
 549 point of the right vortex (see figure 3, right column). A 605
 550 non dimensional vorticity indicator can be constructed, 606
 551 multiplying $\overline{\Omega}$ by the polymer time scale t_{CY} . 607
- 552 • The second indicator is the peak-to-peak amplitude A 609
 553 (difference between maximum and minimum value) of 610
 554 the horizontal profile (along x) for the vertical compo- 611
 555 nent, $\overline{U}_z(x, z = Z_p)$, taken at a given probing altitude 612
 556 Z_p on the fields illustrated figure 3, left column. It is 613

also a measurement of the intensity of the mean flow, but this time associated to the up-going motion. Here we take $Z_p = 2M = 70$ mm, but a similar trend than the one presented hereinafter is observed for different Z_p . This velocity amplitude can be scaled by a grid based reference velocity: the product $f \times S$.

- The last indicator defined here is the position along z of the maximum vertical velocity on the $x = 0$ line (regardless of the value of this velocity). This is an estimation of the area of influence of the mean flow rather than of its intensity and comes as a complement of the two other indicators. It can be further normalized by the mesh parameter M.

The evolution of the peak vorticity magnitude with concentration (indicator 1) is shown in figure 4 and table II. It increases with polymer concentration in the [0-150] ppm range and brutally decreases for the last two points. The critical concentration above which vortex intensity stops increasing, here 150 ppm, can be related to the transition concentration between the dilute and semi-dilute regime, 100 ppm. In the dilute regime, increasing polymer concentration and consequently the solution typical response time leads to an increase in maximum vorticity. When reaching the semi-dilute regime, further increase in concentration on the contrary reduces vorticity associated to mean recirculations. These observation are consistent with the streamline patterns observed in figure 3, central column: well defined structures build up upon polymer addition and grow in the dilute regime, and collapse between 100 and 500 ppm.

In the dilute regime, the characteristic time scale depends on concentration with the scaling $t_{CY} \sim C_{XG}^{1.5}$ (see figure 1). Since here $T = 1/f = 1$ s, scaling based on t_{CY} or De are equivalent. The dimensionless quantity $\overline{\Omega}t_{CY}$ is represented as a function of De (figure 4 b). It follows a power law such that $\overline{\Omega}t_{CY} \sim De^{1.39}$. Since here $t_{CY} \sim De$ (equation 5), it implies that $\overline{\Omega} \sim De^{0.39}$. It should be mentioned that because of the limited range of time scales achievable in the dilute regime (difficulty of making polymer solutions at $C_{XG} < 10$ ppm) and of the single grid frequency used, this scaling is derived from a limited range of De . Larger variations of the Deborah number could be achieved by varying the grid frequency. Yet in the available range, the correlation is quite good. The intensity of mean recirculations increases with the solution time scale, but this increasing rate is reduced as the Deborah number increases (exponent below 1). Mean flow enhancement by polymer addition thus seems to be a low-concentration effect that loses efficiency approaching the semi-dilute regime. This may be explained by the fact that as the relaxation time increases with polymer concentration, viscosity also does. In the dilute regime, the zero shear rate viscosity scales as $C_{XG}^{1.6}$ (from figure 1 b)), hence it increases more rapidly than the relaxation time scale. In the semi-dilute regime, viscosity keeps increasing with the same trend but t_{CY} stays constant (note that Wyatt and Liberatore⁷⁶ observed a change of slope for the semi-dilute regime that is not observed here since no C_{XG} value is used in this domain). In that sense, it may be assumed that viscosity and time scale increase would have two differ-

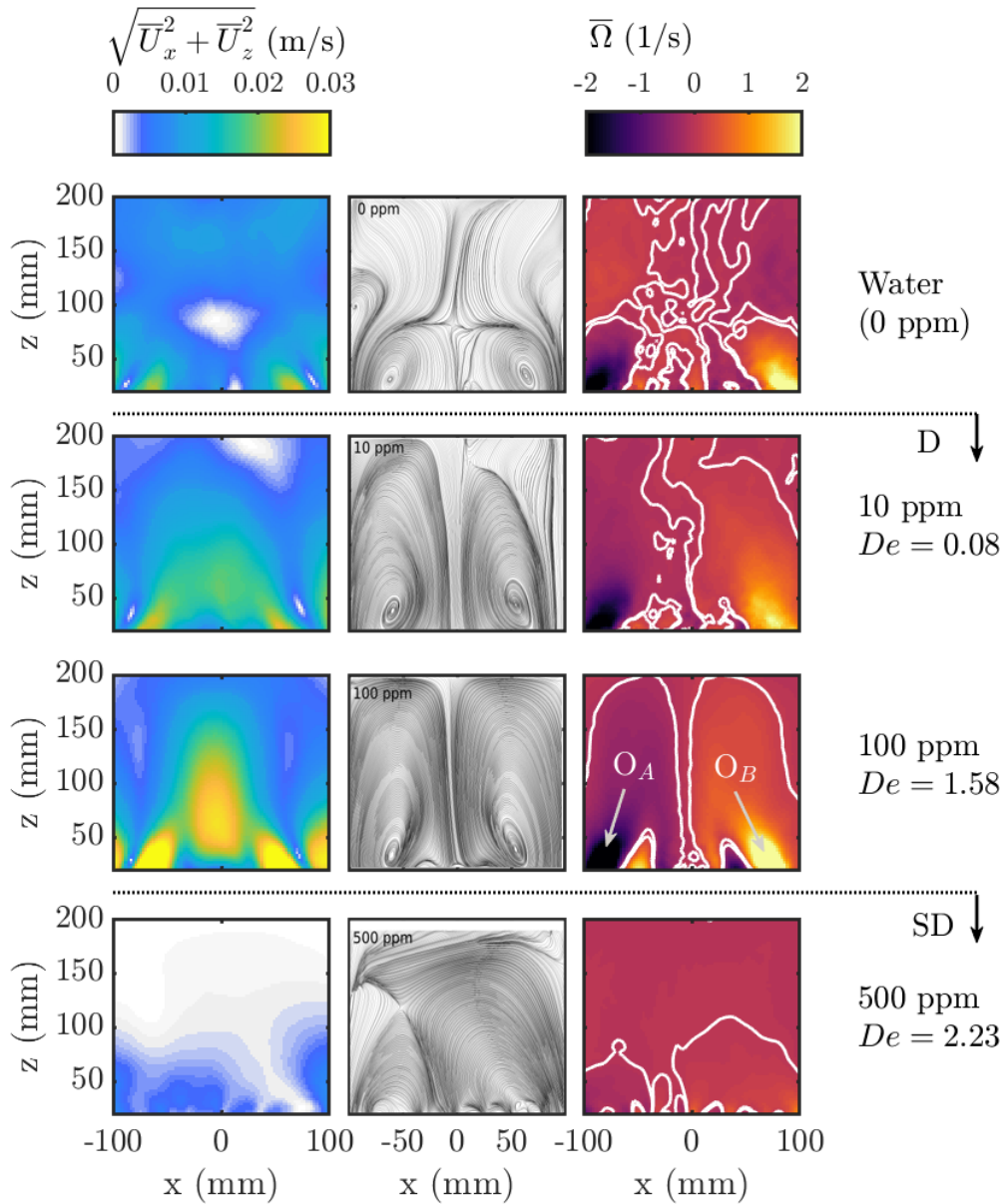


Figure 3. Mean flow inside the grid stirred tank at different XG concentrations. Left column: norm of the 2D mean velocity field $\sqrt{\overline{U}_x^2 + \overline{U}_z^2}$ in m/s. Central columns: streamlines of the mean flow. Right column: Vorticity of the mean velocity field $\overline{\Omega} = \nabla \wedge \overline{\mathbf{U}}$, with contour lines drawn at 2% of the maximum vorticity value.

ent and maybe opposite effects on mean flows: the increase of the solution's time scale seems to enhance re-circulations, whereas increasing viscosity tends to dissipate the flow structures and ultimately make them collapse.

A similar trend is observed when looking at the evolution of the second criterion with polymer concentration: the peak-to-peak amplitude A of the horizontal profile for the vertical velocity component, probed at $z = Z_p = 2M$, $\overline{U}_z(x, 2M)$. Figure

5 a) shows that polymer addition tends to promote a central up-going effect: the $\overline{U}_z(x, 2M)$ black dotted curve for water does not have its maximum value close to $x = 0$ mm, while it is the case for every polymer solutions at any concentrations. This peak effect is increased with polymer concentration until it reaches its maximum for $C_{XG} = 100$ ppm. The indicator A is defined as the curves' "peak-to-peak amplitude", that is to say the difference between the maximum and the minimum values

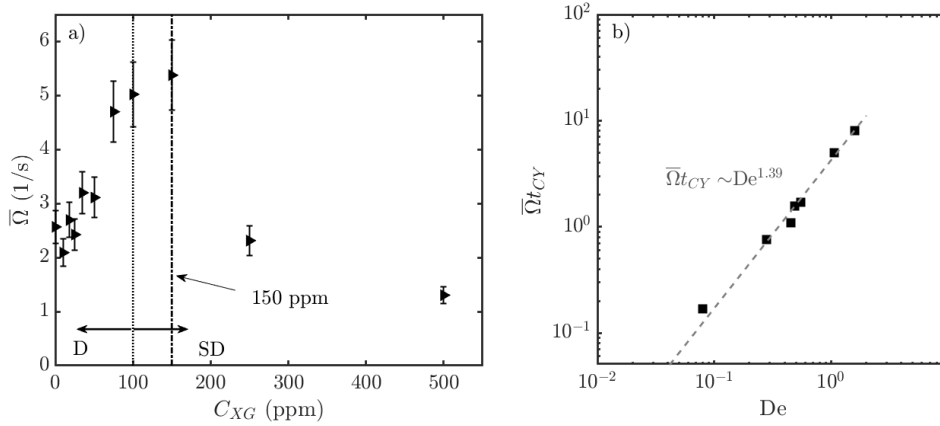


Figure 4. Evolution of vorticity "strength" associated to mean flow structures as a function of polymer concentration and Deborah number. Plot a) is the maximum vorticity $\bar{\Omega}$ between the two counter-rotatives vortex plotted for all concentrations. The relative uncertainty is estimated to be less than $\pm 12\%$, coming from the uncertainties on velocity measurement and from the spatial uncertainty on the location of O_A and O_B . Plot b) shows the non-dimensional quantity $\bar{\Omega}t_{CY}$ in the extended dilute regime ($C_{XG} \leq 100$ ppm left of dashed dotted line in a)). The dotted line in a) denotes the transition between dilute (D) and semi-dilute (SD) concentration regimes, and the dashed dotted marks line in a) the change in trend at $C_{XG} = 150$ ppm. The gray dashed line in b) is the power law fitting of $\bar{\Omega}t_{CY}$ versus De , the scaling of which is reported in b) on top of the curve.

630 of $\bar{U}_z(x, 2M)$ along x , sketched by the dashed arrow on figure
 631 5 a). It is plotted as a function of the polymer concentration
 632 in figure 5 c). An increase compared to the water case is ob-
 633 served for all polymer solutions in the dilute regime. Indicator
 634 A seems to slightly increase with De within this dilute regime,
 635 even though the error bars on the data are also compatible with
 636 a constant A trend. It then collapses in the semi-dilute regime.
 637 This confirms that the intensity of the up-going central motion
 638 and that of the side vortices are coupled, and that they are both
 639 related to the polymer entanglement concentration regime.

640 The third indicator is illustrated by figures 5 b) and d). The
 641 vertical profiles of vertical velocity at $x = 0$ mm plotted in
 642 figure 5 b) all present a maximum value at small z (close to
 643 the grid). Yet, the $z = Z_m$ location of this maximum varies
 644 with polymer concentration. This can also be observed on the
 645 average velocity fields in figure 3, left column, and is a conse-
 646 quence of the flow organization into two side vortices. The
 647 impact region of both vortex meet in the plane of symmetry
 648 ($X = 0$ mm). Since the vortex are ellipsoidal and that their
 649 main axis is neither vertical nor horizontal, the maximum verti-
 650 cal velocity is found at a given altitude which depends on the
 651 inclination of the vortices and their topology. This third cri-
 652 terion thus evaluates the vortex pair's spatial influence more
 653 than their intensity. The altitude at which maximal vertical
 654 velocity is found Z_m is plotted versus concentration in figure 5
 655 d). It shows an increasing trend in the early part of the dilute
 656 regime. However unlike the up-going intensity A , it begins
 657 to decrease at a lower typical concentration, around 35 or 50
 658 ppm.

659 Scaled second and third indicators can be plotted versus
 660 the Deborah number in the dilute regime. The evolution of
 661 A scaled by a reference grid velocity fS is shown in figure 5
 662 e), and that of Z_m scaled by the mesh parameter M in figure
 663 5 f), both in log-log scales. The first plot shows that as for

664 $\bar{\Omega}t_{CY}$, $A/(fS)$ increases with the Deborah number, but on a
 665 very limited range. Figure 5f) seems to confirm the existence
 666 of a critical concentration within the dilute regime: a peak of
 667 Z_m/M is observed precisely at $De = 0.55$ corresponding to
 668 $C_{XG} = 50$ ppm, even if the relative variations of Z_m/M are
 669 quite small in the studied De range.

670 One can quickly comment on the uncertainties of the plots
 671 in figure 5. In a) and b), the relative uncertainty on veloc-
 672 ity value along these profiles is typically equivalent to that on
 673 mean velocity, *i.e.* about $\pm 6\%$. Hence the relative uncertainty
 674 on A and $A/(fS)$ is twice that value, about $\pm 12\%$. The ab-
 675 solute uncertainty on Z_m points in d) would be evaluated as
 676 ± 1.15 mm (from the PIV spatial resolution), which gives a
 677 relative uncertainty on Z_m and Z_m/M less than 3%.

678 The effects of polymer addition and polymer concentration
 679 on mean flows inside the tank can thus be summarized as fol-
 680 lows:

- 681 • Polymer addition has an organizing effect on the mean
 682 flow. Existing vortices are enhanced by addition of even
 683 a small concentration of polymer, and the flow orga-
 684 nizes into two distinct vorticity regions ruled by the pair
 685 of counter rotative eddies. A global up-going motion
 686 appears at the center of the tank.
- 687 • Increasing polymer concentration while staying in the
 688 dilute regime tends to increase the vortex and up-
 689 going motion intensity. Both indicators for vortex
 690 and up-going motion intensity increase until concentra-
 691 tion reaches the critical concentration $C_{XG} = 100$ ppm
 692 for which solution switches from dilute to semi-dilute
 693 regimes. In the concentration range corresponding to
 694 the dilute regime, the maximum vorticity of the mean
 695 flow scales as a power law of the Deborah number.
- 696 • The region of influence of the mean flow is observed to

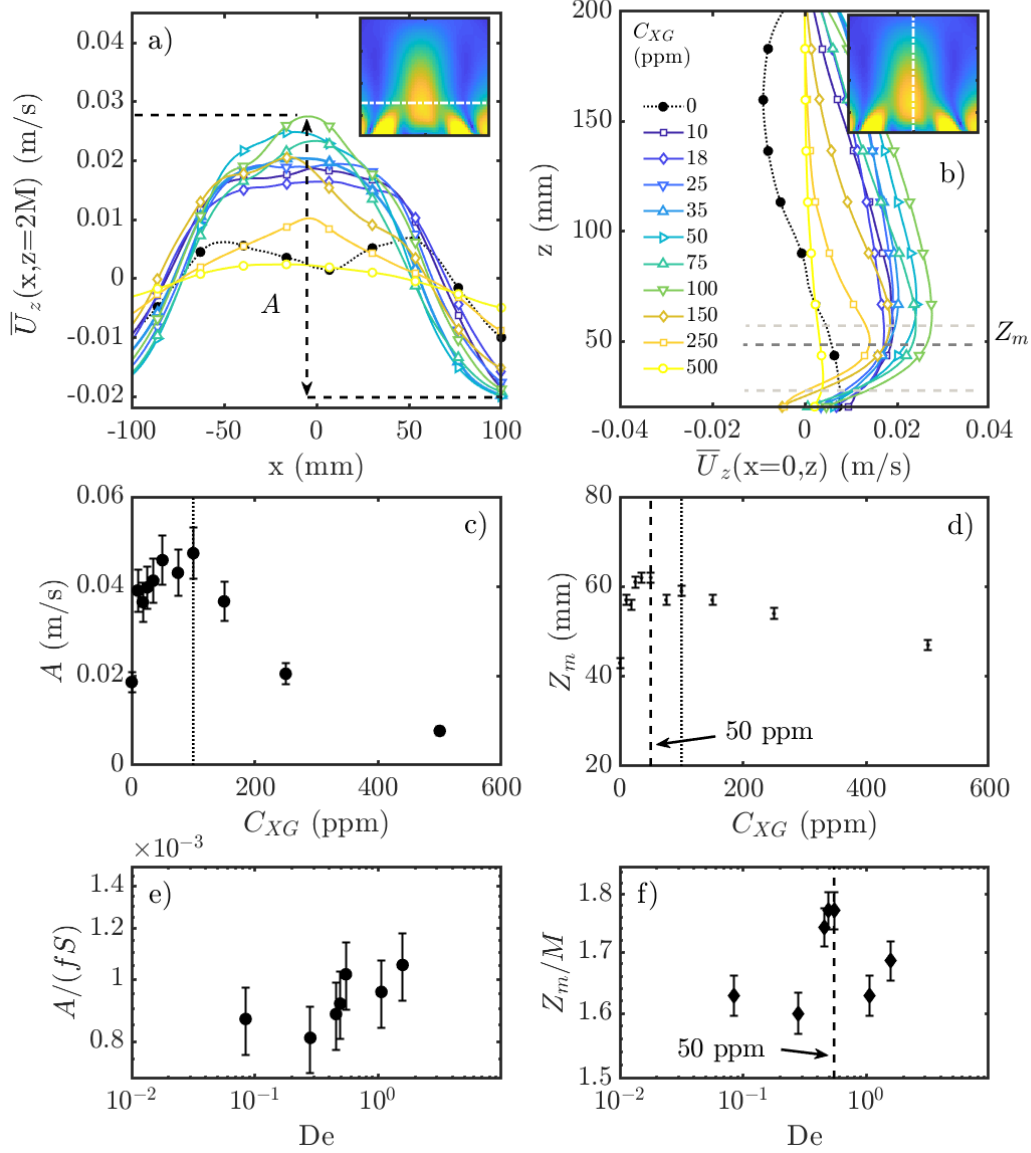


Figure 5. Effect of polymer concentration on vertical velocity. a) Horizontal profiles of the vertical velocity at $z = 2M = 70$ mm. Horizontal dashed lines and the vertical dashed arrow illustrate the peak-to-peak amplitude A indicator. b) Vertical profiles of the vertical velocity at $x = 0$ mm. Gray horizontal dashed lines are examples of $z = Z_m$ depths for profile maxima. Inserts in a) and b) sketch the line along which profiles are plotted by a white dashed line, taking as an example the $C_{XG} = 100$ ppm average velocity field magnitude. Markers in a) and b) are represented for only one in ten data points, for the sake of readability. c) Peak-to-peak amplitude A of the profiles of a). d) location Z_m along z of the maxima of profiles b) (marker size is reduced so that the error bar can be seen). e) and f) show the evolution with De in the dilute regime of the two previous indicators, respectively A and Z_m , scaled by respectively fS and M (in log scale). The dotted lines in c) and d) denote the dilute to semi-dilute entanglement transition ($C_{XG} = 100$ ppm). The black dashed line in d) and f) corresponds to the sub-dilute critical concentration $C_{XG} = 50$ ppm.

697 increase at the onset of polymer addition, but the maximum effect of the up-going motion is attained at a concentration lower than the dilute to semi-dilute transition. This suggests that the dilute regime is itself composed of two sub-regimes: a very dilute one in which both vortex intensity and size increase, and a transition

698
699
700
701
702

to semi-dilute one in which the vortex intensity keeps increasing but its region of influence reduces.

- In the semi-dilute domain, vortex intensity and size both decrease. The hypothesis is that in this regime, viscosity keeps increasing upon polymer addition while elas-

708 ticity of the polymer chains is limited because of emerg-
709 ing polymer-polymer interactions.

710 B. Turbulence properties

711 Turbulence properties are evaluated in the central region of
712 the ROI, where they are the most homogeneous⁴² by cropping
713 out bands for $x > 2.5M$ and $x < -2.5M$ on the sides of the
714 ROI before width averaging quantities (along x) and plotting
715 vertical profiles (along z). This central region is illustrated in
716 figure 6 where two examples (water and 25 ppm XG) of tur-
717 bulent kinetic energy fields k , computed as $k = u_z'^2 + 2u_x'^2$, are
718 shown in log scale. Note that the kinetic energy is computed
719 under an assumption of horizontal isotropy. In the following
720 analysis, all profiles are plotted versus the unscaled dimension
721 z in order to compare with dimensional HT and TT relation-
722 ships for OGT (equations 1, 2).

723 1. Decay of turbulence intensity

724 Profiles of u_x' as a function of z are shown in figure 7 a).
725 For $C_{XG} < 250$ ppm, it appears that all the profiles, water
726 and polymer solutions, follow a power law of constant expo-
727 nent as predicted by the relationship of Hopfinger and Toly⁴
728 (equations 1). The first important observation is thus that the
729 decay of turbulence intensity of OGT in the dilute regime of
730 polymer solutions can be described by "HT-like" profiles. The
731 influence of polymer concentration on this decay is quantified
732 by the power law exponent. In the picture of Hopfinger and
733 Toly⁴, u_x' and u_z' should be proportional, resulting in a single
734 value of n . Following this hypothesis, this value is estimated
735 for each concentration by fitting both the u_x' and u_z' (not shown
736 here) profiles with power laws, and averaging the two result-
737 ing exponents. The difference between these two exponents
738 yields the dispersion bars represented on figure 7 (correspond-
739 ing to the uncertainties in table II).

740 Values of n are reported in table II and plotted versus con-
741 centration in figure 7 b) (for the whole $C_{XG} < 250$ ppm range)
742 and c) (zoomed on $C_{XG} < 100$ ppm). It appears that the
743 n value for water is slightly above the $n=-1$ expected from
744 HT. When adding polymer n starts increasing up to -0.716 at
745 18 ppm (figure 7 c)) before decreasing again, quasi linearly
746 with polymer concentration, until $C_{XG} = 150$ ppm, where it
747 is equal $n = -1.479$. The decay rate of oscillating grid tur-
748 bulence thus varies with polymer concentration, staying quite
749 similar to the water case as long as one stays in the dilute
750 regime.

751 In the semi-dilute regime, the decay of turbulence departs
752 from the HT behavior: the last two concentrations exhibit two
753 asymptotic slopes separated by a transition area, a first one n' ,
754 at small z , which keeps decreasing with increasing C_{XG} but
755 not following the linear trend of n , and a second one $n''=0$
756 at large z . In this second region, turbulent velocity fluctua-
757 tions are extremely small and the mean flow is low as well
758 (see figure 3). Viscous dissipation reduces the velocity mag-
759 nitudes, hence the local shear rate, which further increases

760 viscosity and consequently the dissipation (negative n). This
761 accumulated effect makes the fluid practically turbulence-free
762 and motionless, which is in some ways equivalent to a cavern
763 effect observed in stirred tanks⁷⁸.

764 2. Mean flow to turbulence ratio

765 A key quantity of oscillating grid turbulence is the local
766 mean to turbulence ratio $\Gamma_{ij} = \frac{|\bar{U}_i|}{u_j'}$, between the local abso-
767 lute value of mean velocity component $|\bar{U}_i|$ and the local rms
768 of turbulent velocity fluctuations component u_j' , with $i=x,y$ or
769 z . Γ_{ij} is a 9 component tensor, which reduces to a 4 compo-
770 nent tensor with $i, j = x$ or z for 2D PIV measurements. Most
771 of the time, the values used to estimate the efficiency of a de-
772 vice in terms of turbulence versus mean flow production are
773 diagonal values Γ_{ii} . Here we compute the indicator Γ as the
774 width average of the quantity $(\sum_i \Gamma_{ii}^2)^{0.5}$. For OGT in water, a
775 review by Variano, Bodenschatz, and Cowen⁷⁷ reports local
776 typical best case values of $\Gamma_{ii} = 0.25$ in a single coordinate
777 direction. Here, figure 8 shows that width averaged Γ lies be-
778 tween 0.9 and 3.5 for all fluids. It yet has to be mentioned
779 that mean flow over turbulence ratio can locally reach higher
780 values of up to 10 in the central region where the mean flow is
781 very strong, and down to 0.1 in high turbulence intensity / low
782 mean flow regions. Γ globally increases with polymer concen-
783 tration, which is a consequence of both the enhancement of
784 the mean flow and the decrease of turbulence intensity. Three
785 distinct regions can be seen on the plot of Γ versus z . The
786 first one (1), for $z < M$ and in which $\Gamma < 2$, lays just below
787 the main mean flow structure detailed previously. The second
788 one (2) between $z = M$ and $z = 4M$ corresponds to the region
789 of the up-going motion and side recirculations, and yields the
790 highest Γ values going along with the strongest mean flows.
791 In regions (1) and (2), Γ is always the lowest for water. The
792 third region (3) corresponds to the distances not reached by
793 the principal mean flow structure in polymer solutions, or in
794 which their intensity is reduced, but where turbulence keeps
795 decaying. The values of Γ in the far grid region (3) depend
796 on the existence or not of secondary re-circulations under the
797 free surface. They are comparable to those found for water
798 and can even be lower than in water in some dilute polymer
799 solutions. In region (3), mean flow intensity is at worst twice
800 that of turbulence, no matter the working fluid.

801 3. Integral length scales

802 The integral length scales of turbulence L_{ij}^k are defined as
803 the integral of correlation coefficients of velocity fluctuation
804 components i and j along dimension k , with i, j or $k = x$ or z .
805 They are averaged over sampling regions at different depths.
806 Length scales along x are computed on sampling regions wide
807 as the ROI and including 3 vectors in the z direction. Length
808 scales along z are computed on sampling regions of width
809 equal to that of the ROI's and 10 mm height. The study of
810 integral scales is limited to the dilute regime. As for mean

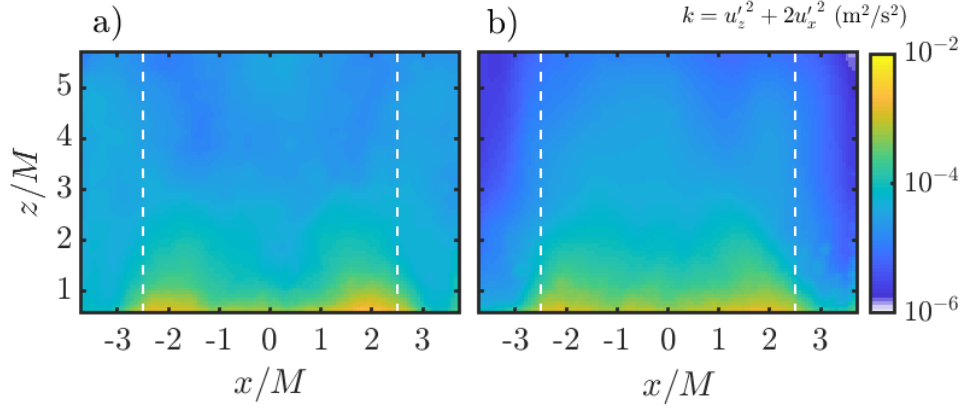


Figure 6. Fields of turbulent kinetic energy $k = u_z'^2 + 2u_x'^2$ in log scale for water (a) and 25 ppm XG solution. Vertical dashed lines at $x/M = \pm 2.5$ denote the boundaries of the domain for horizontally averaged turbulence properties.

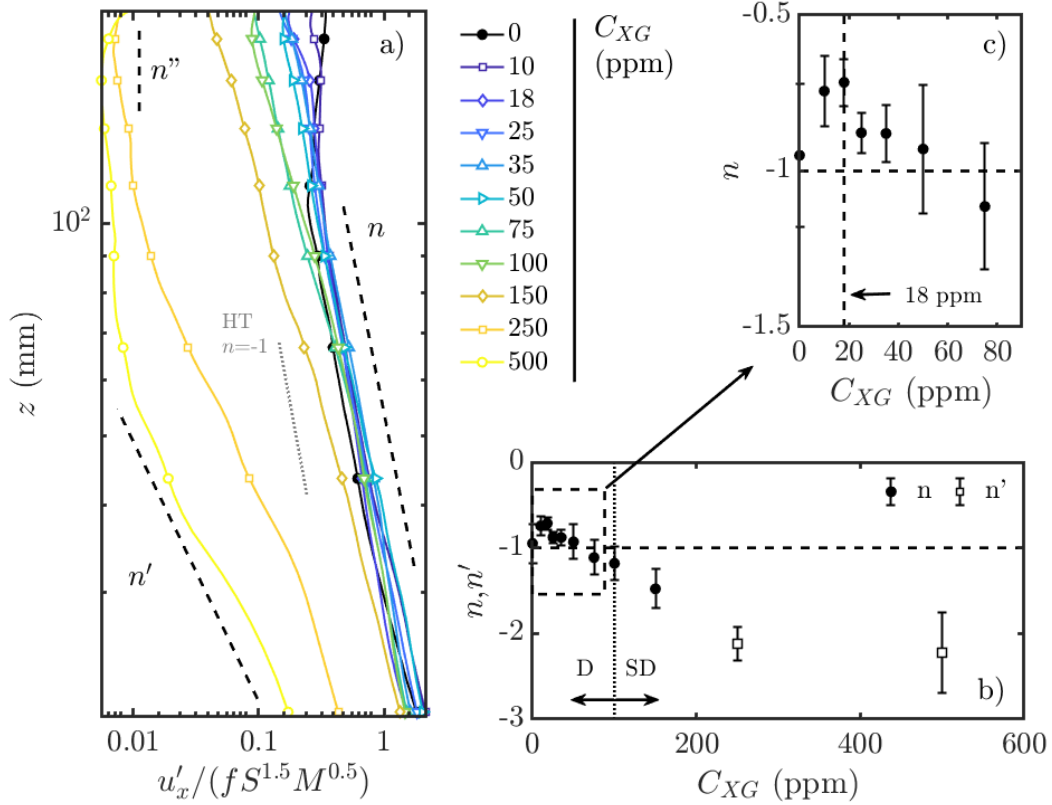


Figure 7. "HT-like" plots of u_x' as a function of z (a), and estimation of the power law exponent evolution as a function of polymer concentration (b). c) is a zoom of b) in the $C_{XG} < 100$ ppm range. Markers in a) are represented for only one in ten data points, for the sake of readability. The typical uncertainty on u_x' is $\pm 5\%$. Vertical bars in b) and c) show the disparity of n measurement from u_x' and u_z' profiles.

811 and rms velocities, uncertainties are estimated by computing
 812 sliding statistics on 500 images samples and evaluating the
 813 variations of the integral length-scales computed from these
 814 samples around the converged value derived from the full data
 815 range. This yields a typical uncertainty of $\pm 10\%$ on horizon-

816 tal scales L_{xx}^x and of $\pm 12\%$ on vertical scales L_{zz}^z .

817 In the definition of Thompson and Turner³, L is equal to the
 818 horizontal scale of horizontal velocity fluctuations L_{xx}^x . Figure
 819 9 shows the evolution of $L = L_{xx}^x$ (a) and of the vertical scale
 820 of vertical velocity fluctuations L_{zz}^z (b) as a function of the

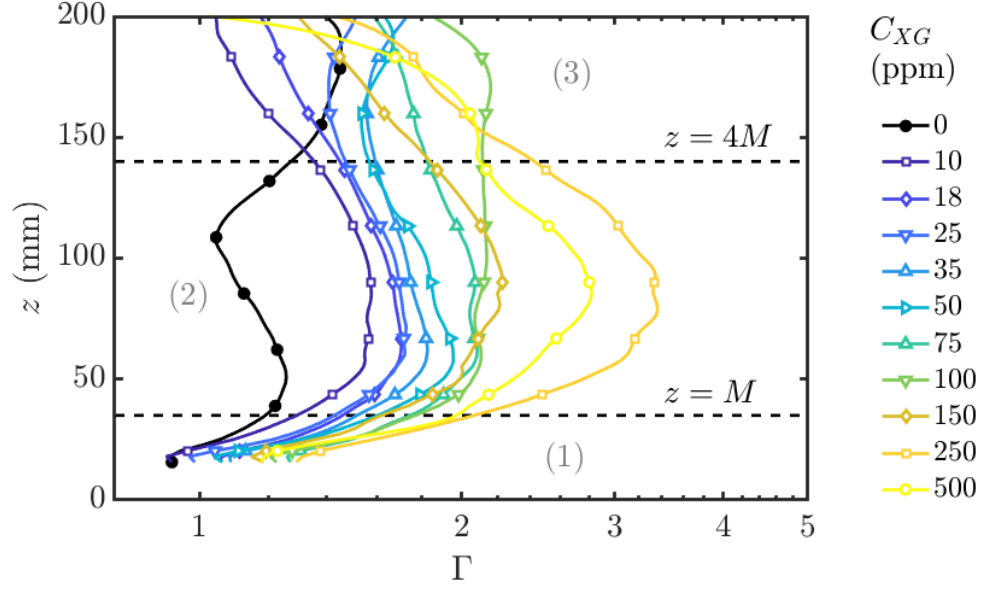


Figure 8. Plots of the mean flow to turbulence indicator Γ , in log scale, as a function of the distance from the grid z . Dashed lines are plotted at $z = M$ and $z = 4M$. Markers are represented for only one in ten data points, for the sake of readability. The typical uncertainty on Γ is $\pm 11\%$, sum of the uncertainties on \bar{U} and u'_x .

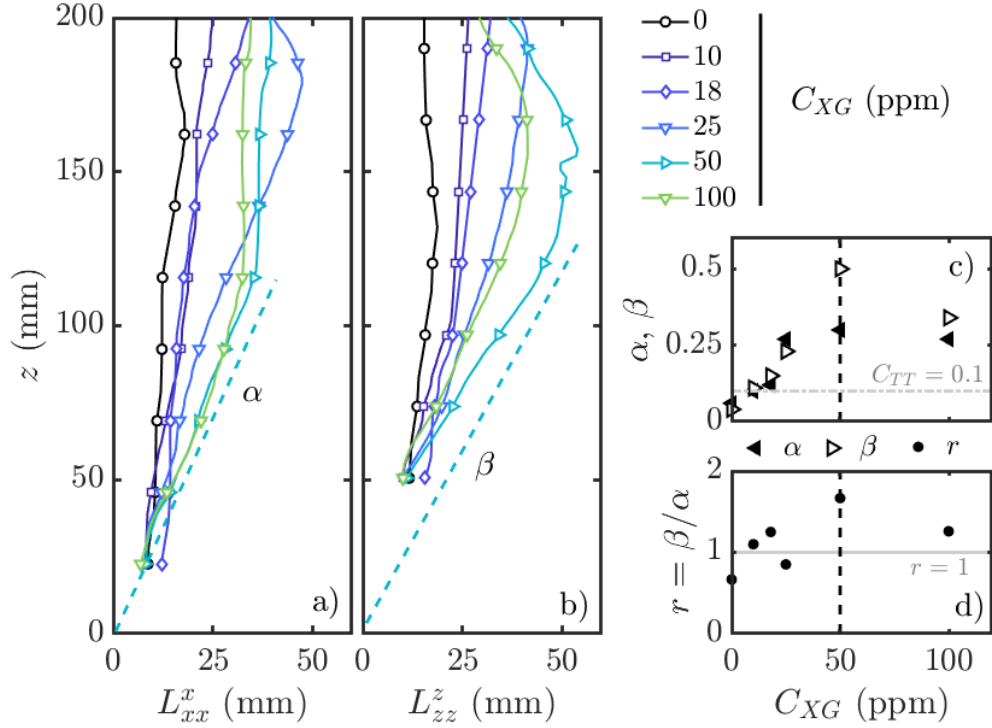


Figure 9. Integral length scales of turbulence in the dilute regime. a) Horizontal scale of horizontal velocity fluctuations L^x_{xx} as a function of the distance to the grid z . b) Vertical scale of vertical velocity fluctuations L^z_{zz} as a function of the distance to the grid z . Markers in a) and b) are represented for only one in ten data points, for the sake of readability. c) Slopes α and β of linear trends of respectively L^x_{xx} and L^z_{zz} at a small z , as a function of polymer concentration. d) Ratio of these two slopes $r = \beta/\alpha$.

821 distance to the grid z . Integral scales are larger in polymer
822 solutions compared to water. This was previously observed in
823 several studies of turbulence in shear-thinning or viscoelastic
824 polymer solutions^{56,59,60}.

825 It appears that up to a given proximity of the free surface,
826 which is located at $z = 250$ mm, both L_{xx}^x and L_{zz}^z scales follow
827 a linear trend with z , as observed by Thompson and Turner³
828 in water. We notice that the change in trend happens at
829 higher depths (smaller z) for the vertical scale L_{zz}^z than for the
830 horizontal one, and that this depth increases with polymer
831 concentration. This is consistent with the fact that vertical
832 velocity structures are kinematically constrained by the hori-
833 zontal interface, and larger for large polymer concentrations
834 (to be detailed in Lacassagne *et al.*⁷⁹).

835 As for the slope of the different linear trends, denoted re-
836 spectively α for L_{xx}^x and β for L_{zz}^z , they are reported in the sub-
837 figure c) of figure 9 and compared with the value predicted by
838 Thompson and Turner³ for water, $C_{TT} = 0.1$. The value of α
839 for $C_{XG} = 0$ is quite close to the expected C_{TT} value. Both α
840 and β increase with polymer concentration up to 50 ppm and
841 seem to initiate a decrease for $C_{XG} > 50$ ppm, meaning that
842 the growth of flow structure moving away from the grid is en-
843 hanced by the presence of polymer at the onset of the dilute
844 regime, and that this enhancement may no longer happen in
845 the semi-dilute one.

846 Finally, the relative evolution of L_{zz}^z and L_{xx}^x can be quan-
847 tified by computing the ratio $r = \beta/\alpha$ at each concentration.
848 $r > 1$ indicates that the vertical dimension of structures in-
849 creases faster than the horizontal one, and $r < 1$ the opposite.
850 Figure 9 d) shows that r is slightly below 1 for water, but
851 increases up to a value of almost 2 for $C_{XG} = 50$ ppm be-
852 fore decreasing again for $C_{XG} = 100$ ppm. The conclusion
853 is that the presence of polymer in the concentration
854 range $C_{XG} \leq 50$ ppm not only enhances the growth of tur-
855 bulence structures moving away from the grid, but also the
856 anisotropy of the growth: the vertical elongation of eddies is
857 promoted. Both behaviours yet seem to reduce when approach-
858 ing the semi-dilute regime.

859 4. Isotropy

860 For OGT in water, it is known that the vertical component
861 of turbulence is stronger than the horizontal one, because this
862 is the orientation of the grid forcing. Hence OGT is by nature
863 not fully isotropic in a vertical plane. An indicator of the 2D
864 isotropy of turbulence in the (\vec{x}, \vec{z}) plane, I_s , can be defined
865 by dividing the HT profiles of the vertical component by the
866 horizontal one: $I_s = u'_z/u'_x$.

867 The I_s indicator is as expected generally above 1, thus con-
868 firming that the vertical velocity fluctuations rms is always
869 larger than the horizontal one, for water and all polymer con-
870 centrations. According to the description of Hopfinger and
871 Toly⁴, the rms of vertical velocity fluctuations should be pro-
872 portional to the rms of horizontal ones with a constant propor-
873 tionality coefficient C_{2HT} . I_s profiles should thus be constant
874 along z , which is here only observed as a first approximation
875 in the dilute regime as will be discussed hereinafter. In this

876 first approximation, the anisotropy coefficient, corresponding
877 to the second HT constant C_{2HT} , can then be obtained for each
878 working fluid as the average of I_s over z (figure 10). In the
879 literature (see section II A 1), its value is between 1.1 and 1.4
880 for water.

881 C_{2HT} is found to increase with polymer concentration (see
882 figure 10 and values reported in table II), first moderately, and
883 then faster above 100 ppm concentrations. The first conclu-
884 sion is thus that the presence of polymer tends to promote
885 turbulence anisotropy, and that this increased anisotropy is all
886 the more important than polymer concentration is high. Yet,
887 for concentrations lower than 100 ppm, the value of HT's sec-
888 ond constant stay inside the range found in the literature for
889 water up to the error bar amplitude, despite the slight increase
890 observed. When entering the semi-dilute regime, that is to say
891 at concentrations above 100 ppm, C_{2HT} increases much faster
892 with concentration.

893 Nevertheless, looking at the evolution of I_s with z , we notice
894 that for polymer solutions, a slight increase of I_s is observed
895 with increasing z . Barely visible at low concentrations, this
896 increase seems all the more important that polymer concen-
897 tration is high, especially for $C_{XG} \geq 250$ ppm. For the two
898 higher concentrations studied, I_s is clearly no longer constant
899 with z . The estimation of C_{2HT} by z -averaging of I_s should
900 thus be interpreted carefully: as long as I_s can be considered
901 constant with z , here to a first approach for $C_{XG} \leq 100$ ppm,
902 the hypothesis of HT holds and anisotropy can be fully de-
903 scribed by the evolution of C_{2HT} . When I_s increases with z ,
904 it means that u'_x and u'_z are no longer proportional, and that
905 u'_z increases faster than u'_x . Hence the HT exponent for u'_z
906 is likely higher than the one for u'_x . Anisotropy is then ex-
907 pressed not only by C_{2HT} but also by the ratio of decay ex-
908 ponents for u'_x and u'_z . Increased anisotropy of turbulence in
909 polymer solutions was already observed by Gupta, Sureshku-
910 mar, and Khomami⁶⁴ or Cai *et al.*⁶³ in channel flows of vis-
911 coelastic polymers, or in turbulent front propagation experi-
912 ments by Cocconi *et al.*⁵⁷. In the first case, it is explained
913 by the ability of polymer chains to align with the mean flow.
914 In the second one, it likely comes from a reorganization of
915 turbulence leading to an alignment of polymers with vortic-
916 ity, which is, as the authors stress out, somehow similar to the
917 mean-flow alignment observed in channel flows. Here, the
918 fact that C_{2HT} is above unity and increases with C_{XG} fits well
919 in this picture: the grid motion being vertical, polymer chains
920 preferentially settle along the periodic vertical shear induced
921 by the grid, and vertical turbulent fluctuations are promoted.
922 The specific behavior observed in the semi-dilute regime has
923 to be tempered by the fact that for such concentrations tur-
924 bulence is very weak, even in the region close to the grid,
925 and transitions to laminar or even motionless in the rest of the
926 tank.

927 As a last remark, one notices that when approaching the
928 free surface (located here at Z close to 250 mm), the previous
929 increasing trend of I_s with z is reversed, the values of I_s de-
930 crease. This suggests that the free surface damps the vertical
931 fluctuations of turbulence more efficiently than the horizontal
932 ones (see Lacassagne *et al.*⁷⁹). Not accounted for by the laws
933 of⁴, this could translate by a strong differentiation of the two

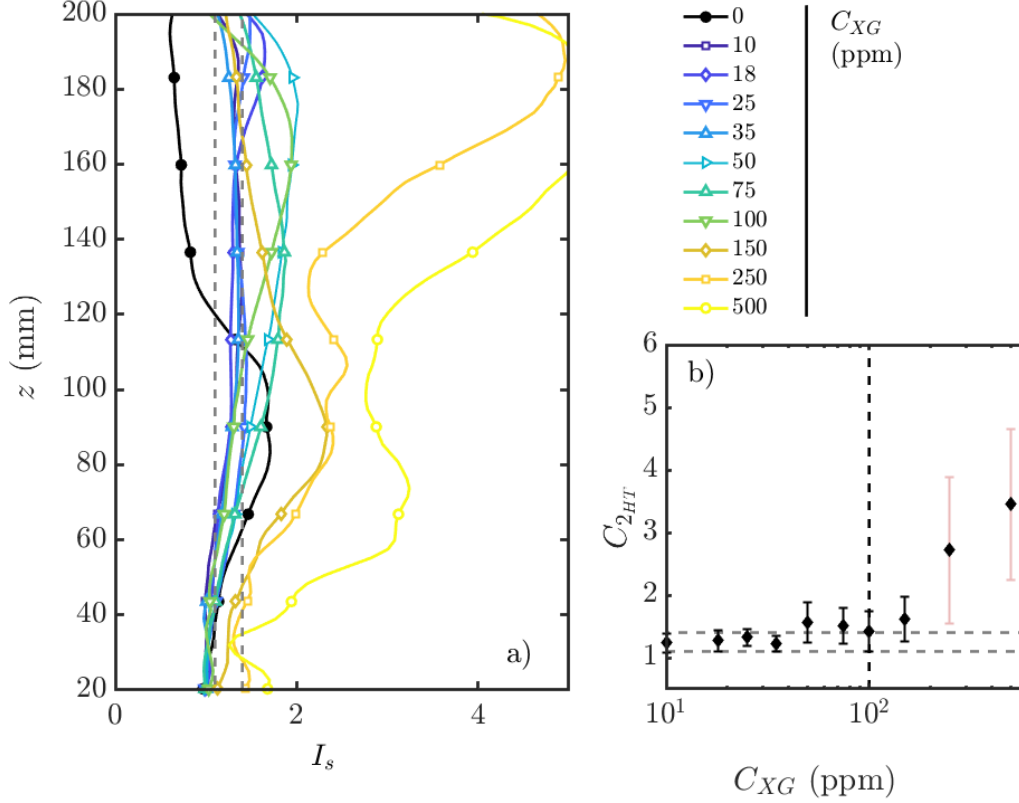


Figure 10. Vertical profiles of anisotropy I_s for water and polymer solutions at different concentrations. a) I_s Isotropy profiles. The typical uncertainty on I_s is twice that of u'_x or u'_z profiles, i.e. $\pm 10\%$. b) Evolution of C_{2HT} , computed as the average of I_s over z , with polymer concentration. Dashed lines are boundaries of the usual range of values found for water $1.1 < C_{2HT} < 1.4$. Vertical bars represent standard deviation of C_{2HT} along z around its average value for each concentration. Markers in a) are represented for only one in ten data points, for the sake of readability.

934 power law exponents for u'_x and u'_z .

935 5. Homogeneity

936 Finally, in order to measure horizontal homogeneity, we de-
 937 fine the quantity H_j^x as the standard deviation over an horizon-
 938 tal line at altitude z of the 2D field of rms velocity fluctuations
 939 in dimension j (j being x or z), normalized by the reference
 940 (width averaged) rms u'_j at this depth. The smaller the H_x^x
 941 or H_z^x the higher the homogeneity in dimension x at a given
 942 z . Homogeneity indicators H_z^x or H_x^x do not show any trend
 943 along z . Values of H_z^x averaged over z , denoted H , are re-
 944 ported in table II. Uncertainty on H value is computed as the
 945 standard deviation of H_z^x over z . H does not seem to depend on
 946 polymer concentration. This implies that polymer has a lesser
 947 effect on turbulence homogeneity than on its isotropy. This is
 948 obviously only valid in the central region of the ROI defined
 949 previously, for $-2.5M < x < 2.5M$.

950 V. DISCUSSION

951 A. Concentration regimes and drag reduction

952 Several characteristic polymer concentrations emerge from
 953 the previous results and observations. The different concentra-
 954 tion sub-ranges and their characteristics in terms of mean flow
 955 and turbulence are summarized in figure 11. Apart from the
 956 100 ppm concentration which marks the transition between
 957 the dilute and semi-dilute regime, two specific critical con-
 958 centrations can be evidenced within the dilute regime itself:
 959 $C_{XG} = C_{D1} \simeq 20$ ppm and $C_{XG} = C_{D2} \simeq 50$ ppm. This leads
 960 to three dilute sub-regimes referred to as D0, D1 and D2.

961 The first critical concentration marks the limit of an ex-
 962 tremely dilute behaviour of the polymer corresponding D0 to
 963 the very onset of polymer action on both mean flows and tur-
 964 bulence. It is worth noting that the existence of such turbulent
 965 inner dilute regimes was already evidenced for other polymer
 966 molecules (PEO, with a 25 ppm critical concentration^{29,80}).

967 The second one corresponds to the maximum mean flow
 968 enhancement concentration reached between D1 and D2 (all
 969 mean flow indicators increase between 0 and 50 ppm), and

C_{XG} (ppm)	Re_g	De	$\bar{\Omega}$ (1/s)	-n (* or -n')	C_{2HT}	H
0	2.03×10^3	0	2.57	1.0 ± 0.3	1.1 ± 0.4	0.10 ± 0.03
10	1.56×10^3	0.08	2.01	0.7 ± 0.1	1.2 ± 0.1	0.08 ± 0.02
18	7.43×10^2	0.28	2.69	0.72 ± 0.08	1.1 ± 0.2	0.08 ± 0.02
25	5.10×10^2	0.45	2.42	0.89 ± 0.06	1.3 ± 0.1	0.10 ± 0.03
35	3.00×10^2	0.49	3.20	0.88 ± 0.09	1.2 ± 0.1	0.08 ± 0.02
50	1.85×10^2	0.55	3.10	0.9 ± 0.2	1.6 ± 0.3	0.11 ± 0.02
75	9.26×10^1	1.06	4.70	1.1 ± 0.2	1.5 ± 0.3	0.13 ± 0.01
100	6.18×10^1	1.60	5.02	1.2 ± 0.2	1.4 ± 0.3	0.11 ± 0.03
150	3.74×10^1	1.60	5.37	1.5 ± 0.2	1.6 ± 0.4	0.13 ± 0.03
250*	2.10×10^1	1.60	2.31	2.1 ± 0.2	3 ± 1	0.14 ± 0.04
500*	9.97×10^0	1.60	1.30	2.2 ± 0.5	3 ± 1	0.10 ± 0.06

Table II. Evolution of several properties (De, n, C_{2HT}) and indicators ($\bar{\Omega}$, H) with polymer concentration. H is the average of H_z^x over z.

also to the maximum large turbulent scale enhancement, in an anisotropic fashion (see figure 9). It can be inferred that this state of maximize mean flow, found at 50 ppm, corresponds to a given state of polymer-flow interactions (alignment, ratios between polymer relaxation time-scales and turbulent time scales...). A maximized mean flow would imply that interactions between polymer and small turbulent structures are reduced, and energy transfer towards large scales of the flow are favoured. The question is then the following: since the polymer concentration lies inside the dilute entanglement regime (lower than 100 ppm) for which mechanical interactions between polymer chains is assumed negligible, what then causes polymer chains to exhibit variable response to the flow? A possible explanation is the existence of polymer-polymer electrical interactions. It is indeed known that when transitioning from the dilute to the semi-dilute regime, long chained XG molecules first see each other through repulsive and attractive electrical forces caused by the presence of electrically charged complex on the polymer carbonate backbone⁷⁶. Would this mean that the critical 50 ppm concentration marks the onset of polymer electrical interactions, "smoothing" the dilute to semi-dilute transition? This open question needs to be answered by a coupling between the knowledge of typical flow time-scales, and theoretical models of polymer conformation state and electrical interactions.

It is in that sense interesting to notice that a critical concentration for drag reduction of XG solutions is found quite close, at $C_{XG} = 70$ ppm by Wyatt, Gunther, and Liberatore⁸¹. These previous concentrations can indeed be related to the drag reduction properties (type B) of XG. Wyatt, Gunther, and Liberatore⁸¹ evidenced drag reduction for XG flowing in pipes at XG concentrations down to 20 ppm. Sohn *et al.*⁸² achieved drag reduction by XG in a rotating disk apparatus at concentrations down to 10 ppm, but found a critical concentration for maximum drag reduction at 200 ppm. Pereira, Andrade, and Soares⁸³ observed drag reduction for XG concentration as low as 2 ppm, and a critical concentration at 37.5 ppm below which drag reduction efficiency falls with increasing C_{XG} and above which it increases. They stressed that this last two-trend behavior is significantly different from that of type A drag reducing polymers, for which drag reduction monotonously increases with polymer concentration. These last remarks support our observations that several hydrodynamic sub-regimes of concentration can exist for XG and long chained polymers. As it is the case for drag reducing properties, the values of these critical concentrations should depend on the conformation of the polymer chains, on the presence of salt that may modify this conformation^{84,85}, on the entanglement state, and on the molecular weight of the polymer chains,^{76,83}. The first critical concentration C_{D1} , comparing to low critical drag reduction concentrations, is thus likely related to conformation effects and physical properties of polymer chains. The second, higher, critical concentration C_{D2} could be explainable by mean shear alignment effects. The critical concentration, $C_{XG} = 100$ ppm (and the 100 ppm to 150 ppm transition) is by definition connected to polymer-polymer interactions.

B. Possible mean flow production and feeding mechanisms

In McCorquodale and Munro⁴², a physical explanation of the origin of the mean flow in OGT is proposed. The authors argue that mean flow arises when there is "a significant difference in the relative strengths of the jets produced by the oscillating grid in different regions of the tank", and relate it to a Coanda effect applying on the jets closer to the walls. The authors check that when artificially separating the side jets from the central ones, using an inner box, mean flow intensity is significantly reduced inside that inner box. What can be added to this picture when the working fluid is a shear thinning polymer solution, is the fact that strong shearing of the fluid in the region between the grid and the wall tends to locally reduce the average viscosity on the sides of the tank. Jets induced by the grid motion are thus by nature of even more variable strength depending on their distance from the wall: near wall jets on each side of the tank see a statistically lower viscosity than jets close to $x = 0$. The fact that mean flow is enhanced in presence of polymer in the dilute regime is thus consistent with the mean flow origin proposed by McCorquodale and Munro⁴².

It has also been shown in several studies that the effect of polymer can propagate to larger scales (see section II B). This can translate for example into an increase of integral length scales and of large scale fluctuations of velocity^{56,59,60}. This

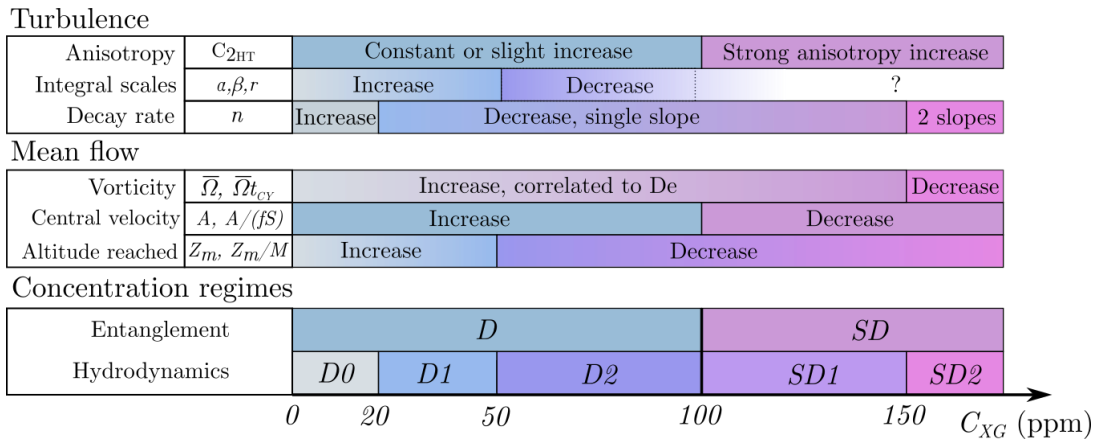


Figure 11. Summary of indicators and flow properties evolution with concentration, and sketch of concentration regimes and sub-regimes.

1051 up-scale energy transfer⁵⁵ could be another feeding mecha- 1088
 1052 nisms for the mean flow, explaining its enhancement with in- 1089
 1053 creasing polymer concentration in the dilute regime. To con- 1090
 1054 firm such an hypothesis, it would be interesting to study turbu- 1091
 1055 lence inside the grid sweep region and try to evidence energy 1092
 1056 transfer terms that could fuel the mean flow. 1093

1057 VI. CONCLUSION AND PERSPECTIVES

1058 In this work, the hydrodynamics in an oscillating grid 1098
 1059 stirred tank filled with either water or shear-thinning XG so- 1099
 1060 lutions have been investigated. It is found that the presence of 1100
 1061 polymer tends to enhance the mean flow in the dilute regime, 1101
 1062 by structuring and increasing the two side recirculations al- 1102
 1063 ready existing in water. This mean flow increase can be related
 1064 to the shear-thinning Deborah number in the dilute regime. In
 1065 the semi-dilute regime, the further increase of viscosity not
 1066 being followed by an increase in De leads to a collapse of the
 1067 mean flow. As for turbulence, its properties also evolve with
 1068 polymer concentration, especially its decay rate, its isotropy,
 1069 and the size of its largest turbulent structures. In the dilute
 1070 regime, the HT and TT descriptions of OGT in water can be
 1071 adapted to shear thinning XG solutions. 1109

1072 Oscillating grid apparatus can thus be used as tools to gen- 1110
 1073 erate controlled turbulence in dilute regime shear thinning 1111
 1074 polymer solutions. In this concentration range, laws for OGT 1112
 1075 in dilute polymer solutions can be compared to those in water. 1113
 1076 A non-negligible mean flow has to be accounted for, but it is
 1077 mostly acting in the bulk flow of OGT in the $z < 4M$ region. 1114
 1078 Mean flow over turbulent intensity levels remain comparable 1115
 1079 closer to the free surface for $z > 4M$, making it possible to 1116
 1080 study turbulence, mixing and mass transfer boundary layers 1117
 1081 in such fluids, as done in water. 1118

1082 The overall evolution of hydrodynamic properties with 1119
 1083 polymer concentration can be described by several critical 1120
 1084 concentrations, splitting the dilute and semi-dilute entangle- 1121
 1085 ment regimes into several hydrodynamic sub-regimes. In par- 1122
 1086 ticular, it is worth noting that transition exist at concentrations 1123
 1087 as low as about $C_{XG} \simeq 20$ ppm, comparable to critical con- 1124

1088 centrations for drag reduction. A more extensive characteri-
 1089 zation of turbulence properties would come from a parametric
 1090 study of the influence of f , S or M on the velocity and integral
 1091 scales of turbulence. This could for example allow to discus-
 1092 s the value of C_{1HT} in polymer solutions, and its possible
 1093 dependency on Re_g . Three-dimensional effects in turbulence
 1094 and mean flow could be investigated by either additional PIV
 1095 measurements in other planes of the tank, or directly by us-
 1096 ing three-dimensional particle tracking methods. Finally the
 1097 mechanisms of turbulence and mean flow production at the
 1098 grid level remain to be fully understood. Interesting data could
 1099 be brought by velocity measurements inside the grid sweep
 1100 region, and by the study of energy fluxes transferred between
 1101 oscillating motion induced by the grid, turbulence, and mean
 1102 flow structures.

1103 REFERENCES

- 1104 ¹M. W. McCorquodale and R. J. Munro, "Experimental study of oscillating-
 1105 grid turbulence interacting with a solid boundary," *Journal of Fluid Me-*
 1106 *chanics* **813**, 768–798 (2017).
- 1107 ²M. W. McCorquodale and R. J. Munro, "Analysis of intercomponent energy
 1108 transfer in the interaction of oscillating-grid turbulence with an imperme-
 1109 able boundary," *Physics of Fluids* **30**, 015105 (2018).
- 1110 ³S. M. Thompson and J. S. Turner, "Mixing across an interface due to tur-
 1111 bulence generated by an oscillating grid," *Journal of Fluid Mechanics* **67**,
 1112 349–368 (1975).
- 1113 ⁴E. J. Hopfinger and J.-A. Toly, "Spatially decaying turbulence and its re-
 1114 lation to mixing across density interfaces," *Journal of Fluid Mechanics* **78**,
 1115 155–175 (1976).
- 1116 ⁵E. Xuequan and E. J. Hopfinger, "On mixing across an interface in stably
 1117 stratified fluid," *Journal of Fluid Mechanics* **166**, 227–244 (1986).
- 1118 ⁶L. Verso, M. van Reeuwijk, and A. Liberzon, "Steady state model and ex-
 1119 periment for an oscillating grid turbulent two-layer stratified flow," *Physical*
 1120 *Review Fluids* **2**, 104605 (2017).
- 1121 ⁷Y. Nagami and T. Saito, "An Experimental Study of the Modulation of
 1122 the Bubble Motion by Gas-Liquid-Phase Interaction in Oscillating-Grid
 1123 Decaying Turbulence," *Flow, Turbulence and Combustion* **92**, 147–174
 1124 (2013).
- 1125 ⁸L. San, T. Long, and C. C. K. Liu, "Algal Bioproductivity in Turbulent
 1126 Water: An Experimental Study," *Water* **9**, 304 (2017).
- 1127 ⁹M. Rastello, H. Michallet, and J.-L. Marié, "Sediment erosion in zero-
 1128 mean-shear turbulence," *Coastal Dynamics*, 597–607 (2017).
- 1129 ¹⁰M. T. Mahamod, W. H. M. W. Mohtar, and S. F. M. Yusoff, "Spatial and

- temporal behavior of pb, cd and zn release during short term low intensity resuspension events," *Jurnal Teknologi* **80** (2017).
- ¹¹R. Vonlanthen and P. A. Monkewitz, "Grid turbulence in dilute polymer solutions: PEO in water," *Journal of Fluid Mechanics* **730**, 76–98 (2013).
- ¹²B. H. Brumley and G. H. Jirka, "Near-surface turbulence in a grid-stirred tank," *Journal of Fluid Mechanics* **183**, 235–263 (1987).
- ¹³S. P. McKenna and W. R. McGillis, "The role of free-surface turbulence and surfactants in air–water gas transfer," *International Journal of Heat and Mass Transfer* **47**, 539–553 (2004).
- ¹⁴H. Herlina, *Gas transfer at the air-water interface in a turbulent flow environment*, Ph.D. thesis, Universitätsverlag Karlsruhe, Karlsruhe (2005).
- ¹⁵L. Chiapponi, S. Longo, and M. Tonelli, "Experimental study on oscillating grid turbulence and free surface fluctuation," *Experiments in Fluids* **53**, 1515–1531 (2012).
- ¹⁶J. Magnaudet, "High-Reynolds-number turbulence in a shear-free boundary layer: revisiting the Hunt–Graham theory," *Journal of Fluid Mechanics* **484**, 167–196 (2003).
- ¹⁷J. Magnaudet and I. Calmet, "Turbulent mass transfer through a flat shear-free surface," *Journal of Fluid Mechanics* **553**, 155–185 (2006).
- ¹⁸H. Herlina and J. G. Wissink, "Direct numerical simulation of turbulent scalar transport across a flat surface," *Journal of Fluid Mechanics* **744**, 217–220 (2014).
- ¹⁹H. Herlina and G. H. Jirka, "Experiments on gas transfer at the air–water interface induced by oscillating grid turbulence," *Journal of Fluid Mechanics* **594**, 183–208 (2008).
- ²⁰J. G. Janzen, H. Herlina, G. H. Jirka, H. E. Schulz, and J. S. Gulliver, "Estimation of mass transfer velocity based on measured turbulence parameters," *AIChE Journal* **56**, 2005–2017 (2010).
- ²¹D. E. Turney and S. Banerjee, "Air–water gas transfer and near-surface motions," *Journal of Fluid Mechanics* **733**, 588–624 (2013).
- ²²E. A. Variano and E. A. Cowen, "Turbulent transport of a high-Schmidt-number scalar near an air–water interface," *Journal of Fluid Mechanics* **731**, 259–287 (2013).
- ²³T. Lacassagne, M. EL Hajem, F. Morge, S. Simoëns, and J.-Y. Champagne, "Study of Gas Liquid Mass Transfer in a Grid Stirred Tank," *Oil & Gas Science and Technology – Revue d'IFP Energies nouvelles* **72**, 7 (2017).
- ²⁴H. Herlina and J. G. Wissink, "Isotropic-turbulence-induced mass transfer across a severely contaminated water surface," *Journal of Fluid Mechanics* (2016).
- ²⁵J. G. Wissink, H. Herlina, Y. Akar, and M. Uhlmann, "Effect of surface contamination on interfacial mass transfer rate," *Journal of Fluid Mechanics* **830**, 5–34 (2017).
- ²⁶Y. Kawase, B. Halard, and M. Moo-Young, "Theoretical prediction of volumetric mass transfer coefficients in bubble columns for Newtonian and non-Newtonian fluids," *Chemical Engineering Science* **42**, 1609–1617 (1987).
- ²⁷M. Jimenez, N. Dietrich, J. R. Grace, and G. Hébrard, "Oxygen mass transfer and hydrodynamic behaviour in wastewater: Determination of local impact of surfactants by visualization techniques," *Water Research* **58**, 111–124 (2012).
- ²⁸A. de Lamotte, A. Delafosse, S. Calvo, F. Delvigne, and D. Toye, "Investigating the effects of hydrodynamics and mixing on mass transfer through the free-surface in stirred tank bioreactors," *Chemical Engineering Science* **172**, 125–142 (2017).
- ²⁹A. Liberzon, M. Holzner, B. Lüthi, M. Guala, and W. Kinzelbach, "On turbulent entrainment and dissipation in dilute polymer solutions," *Physics of Fluids (1994-present)* **21**, 035107 (2009).
- ³⁰Y. Wang, W.-H. Cai, T.-Z. Wei, L. Wang, and F.-C. Li, "Experimental Study on Two-Oscillating Grid Turbulence With Polymer Additives," (ASME, Seoul, South Korea, 2015) p. V001T15A008.
- ³¹Y. Wang, W.-H. Cai, T.-Z. Wei, H.-N. Zhang, L. Wang, and F.-C. Li, "Proper orthogonal decomposition analysis for two-oscillating grid turbulence with viscoelastic fluids," *Advances in Mechanical Engineering* **8**, 1687814016679773 (2016).
- ³²S. I. Voropayev and H. J. S. Fernando, "Propagation of grid turbulence in homogeneous fluids," *Physics of Fluids* **8**, 2435–2440 (1996).
- ³³H. J. Rouse and J. Dodu, "Turbulent diffusion across a density discontinuity," *La Houille Blanche*, 522–532 (1955).
- ³⁴M. Bouvard and H. Dumas, "Application de la méthode de fil chaud à la mesure de la turbulence dans l'eau," *La Houille Blanche*, 257–270 (1967).
- ³⁵T. J. McDougall, "Measurements of turbulence in a zero-mean-shear mixed layer," *Journal of Fluid Mechanics* **94**, 409–431 (1979).
- ³⁶R. I. Nokes, "On the entrainment rate across a density interface," *Journal of Fluid Mechanics* **188**, 185–204 (1988).
- ³⁷I. P. D. D. Silva and H. J. S. Fernando, "Some aspects of mixing in a stratified turbulent patch," *Journal of Fluid Mechanics* **240**, 601–625 (1992).
- ³⁸C. R. Chu and G. H. Jirka, "Turbulent gas flux measurements below the air-water interface of a grid-stirred tank," *International Journal of Heat and Mass Transfer* **35**, 1957–1968 (1992).
- ³⁹N. Matsunaga, Y. Sugihara, T. Komatsu, and A. Masuda, "Quantitative properties of oscillating-grid turbulence in a homogeneous fluid," *Fluid Dynamics Research* **25**, 147–165 (1999).
- ⁴⁰W. H. M. Wan Mohtar, "Oscillating-grid turbulence at large strokes: Revisiting the equation of Hopfinger and Toly," *Journal of Hydrodynamics, Ser. B* **28**, 473–481 (2016).
- ⁴¹S. P. McKenna and W. R. McGillis, "Observations of flow repeatability and secondary circulation in an oscillating grid-stirred tank," *Physics of Fluids (1994-present)* **16**, 3499–3502 (2004).
- ⁴²M. W. McCorquodale and R. J. Munro, "A method for reducing mean flow in oscillating-grid turbulence," *Experiments in Fluids* **59**, 182 (2018).
- ⁴³B. A. Toms, "Some observation on the flow of linear polymer solutions through straight tubes at large Reynolds numbers," (J.G. Oldroyd, Scheveningen, 1948) pp. 135–141.
- ⁴⁴E. van Doorn, C. M. White, and K. R. Sreenivasan, "The decay of grid turbulence in polymer and surfactant solutions," *Physics of Fluids (1994-present)* **11**, 2387–2393 (1999).
- ⁴⁵R. H. Nadolink and W. W. Haigh, "Bibliography on Skin Friction Reduction With Polymers and Other Boundary-Layer Additives," *Applied Mechanics Reviews* **48**, 351–460 (1995).
- ⁴⁶J. L. Lumley, "Drag Reduction by Additives," *Annual Review of Fluid Mechanics* **1**, 367–384 (1969).
- ⁴⁷K. R. Sreenivasan and C. M. White, "The onset of drag reduction by dilute polymer additives, and the maximum drag reduction asymptote," *Journal of Fluid Mechanics* **409**, 149–164 (2000).
- ⁴⁸P. S. Virk, "Drag reduction fundamentals," *AIChE Journal* **21**, 625–656 (1975).
- ⁴⁹P. S. Virk and D. L. Waggener, "Aspects of Mechanisms in Type B Drag Reduction," in *Structure of Turbulence and Drag Reduction*, International Union of Theoretical and Applied Mechanics, edited by A. Gyr (Springer, Berlin, Heidelberg, 1990) pp. 201–213.
- ⁵⁰P. S. Virk, "Drag reduction by collapsed and extended polyelectrolytes," *Nature* **253**, 253109a0 (1975).
- ⁵¹M. Tabor and P. G. d. Gennes, "A Cascade Theory of Drag Reduction," *EPL (Europhysics Letters)* **2**, 519 (1986).
- ⁵²M. D. Warholic, H. Massah, and T. J. Hanratty, "Influence of drag-reducing polymers on turbulence: effects of Reynolds number, concentration and mixing," *Experiments in Fluids* **27**, 461–472 (1999).
- ⁵³M. D. Warholic, D. K. Heist, M. Katcher, and T. J. Hanratty, "A study with particle-image velocimetry of the influence of drag-reducing polymers on the structure of turbulence," *Experiments in Fluids* **31**, 474–483 (2001).
- ⁵⁴H.-D. Xi, E. Bodenschatz, and H. Xu, "Elastic Energy Flux by Flexible Polymers in Fluid Turbulence," *Physical Review Letters* **111** (2013).
- ⁵⁵M. Q. Nguyen, A. Delache, S. Simoëns, W. J. T. Bos, and M. EL Hajem, "Small scale dynamics of isotropic viscoelastic turbulence," *Physical Review Fluids* **1**, 083301 (2016).
- ⁵⁶E. De Angelis, C. M. Casciola, R. Benzi, and R. Piva, "Homogeneous isotropic turbulence in dilute polymers," *Journal of Fluid Mechanics* **531**, 1–10 (2005).
- ⁵⁷G. Cocconi, E. De Angelis, B. Frohnafel, M. Baevsky, and A. Liberzon, "Small scale dynamics of a shearless turbulent/non-turbulent interface in dilute polymer solutions," *Physics of Fluids* **29**, 075102 (2017).
- ⁵⁸A. Liberzon, M. Guala, B. Lüthi, W. Kinzelbach, and A. Tsinober, "Turbulence in dilute polymer solutions," *Physics of Fluids* **17**, 031707 (2005).
- ⁵⁹A. Liberzon, M. Guala, W. Kinzelbach, and A. Tsinober, "On turbulent kinetic energy production and dissipation in dilute polymer solutions," *Physics of Fluids* **18**, 125101 (2006).
- ⁶⁰A. Liberzon, "On the effects of dilute polymers on driven cavity turbulent flows," *International Journal of Heat and Fluid Flow* **32**, 1129–1137 (2011).
- ⁶¹A. M. Crawford, N. Mordant, H. Xu, and E. Bodenschatz, "Fluid acceleration in the bulk of turbulent dilute polymer solutions," *New Journal of Physics* **10**, 123015 (2008).

- 1270 ⁶²S. Rahgozar and D. E. Rival, "On turbulence decay of a shear-thinning 1311
1271 fluid," *Physics of Fluids* **29**, 123101 (2017). 1312
- 1272 ⁶³W.-H. Cai, F.-C. Li, H.-N. Zhang, X.-B. Li, B. Yu, J.-J. Wei, Y. Kawaguchi, 1313
1273 and K. Hishida, "Study on the characteristics of turbulent drag-reducing 1314
1274 channel flow by particle image velocimetry combining with proper orthog- 1315
1275 onal decomposition analysis," *Physics of Fluids* **21**, 115103 (2009). 1316
- 1276 ⁶⁴V. K. Gupta, R. Sureshkumar, and B. Khomami, "Passive scalar transport 1317
1277 in polymer drag-reduced turbulent channel flow," *AIChE Journal* **51**, 1938–1318
1278 1950 (2005). 1319
- 1279 ⁶⁵O. Bentata, D. Anne-Archard, and P. Brancher, "Experimental study of low 1320
1280 inertia vortex rings in shear-thinning fluids," *Physics of Fluids* **30**, 113103 1321
1281 (2018). 1322
- 1282 ⁶⁶N. Cagney and S. Balabani, "Taylor-Couette flow of shear-thinning fluids," 1323
1283 *Physics of Fluids* **31**, 053102 (2019). 1324
- 1284 ⁶⁷A. G. Fabula, *An experimental study of grid turbulence in dilute high- 1325
1285 polymer solutions*, Ph.D. thesis, The Pennsylvania State University, Uni- 1326
1286 versity Park, PA (1966). 1327
- 1287 ⁶⁸B. J. S. Barnard and R. H. J. Sellin, "Grid turbulence in dilute polymer 1328
1288 solutions," *Nature*, 1160–1162 (1969). 1329
- 1289 ⁶⁹C. A. Greated, "Effect of Polymer Additive on Grid Turbulence," *Nature* 1330
1290 **224**, 1196–1197 (1969). 1331
- 1291 ⁷⁰C. A. Friehe and W. H. Schwarz, "Grid-generated turbulence in dilute poly- 1332
1292 mer solutions," *Journal of Fluid Mechanics* (1970). 1333
- 1293 ⁷¹W. D. McComb, J. Allan, and C. A. Greated, "Effect of polymer additives 1334
1294 on the small-scale structure of grid-generated turbulence," *The Physics of* 1335
1295 *Fluids* **20**, 873–879 (1977). 1336
- 1296 ⁷²A. B. Rodd, D. E. Dunstan, and D. V. Boger, "Characterisation of xanthan 1337
1297 gum solutions using dynamic light scattering and rheology," *Carbohydrate* 1338
1298 *Polymers* **42**, 159–174 (2000). 1339
- 1299 ⁷³F. Garcia-Ochoa, V. E. Santos, J. A. Casas, and E. Gomez, "Xanthan gum: 1340
1300 production, recovery, and properties," *Biotechnology Advances* **18**, 549– 1341
1301 579 (2000). 1342
- 1302 ⁷⁴T. Lacassagne, *Oscillating grid turbulence and its influence on gas liquid 1343
1303 mass transfer and mixing in non-Newtonian media*, PhD Thesis, University 1344
1304 of Lyon, INSA Lyon (2018). 1345
- 1305 ⁷⁵G. Cuvelier and B. Launay, "Concentration regimes in xanthan gum solu- 1346
1306 tions deduced from flow and viscoelastic properties," *Carbohydrate Poly-* 1347
1307 *mers* **6**, 321–333 (1986). 1348
- 1308 ⁷⁶N. B. Wyatt and M. W. Liberatore, "Rheology and viscosity scaling of the 1349
1309 polyelectrolyte xanthan gum," *Journal of Applied Polymer Science* **114**, 1350
1310 4076–4084 (2009).
- ⁷⁷E. A. Variano, E. Bodenschatz, and E. A. Cowen, "A random synthetic jet 1311
array driven turbulence tank," *Experiments in Fluids* **37**, 613–615 (2004).
- ⁷⁸Q. Xiao, N. Yang, J. Zhu, and L. Guo, "Modeling of cavern formation in 1312
yield stress fluids in stirred tanks," *AIChE Journal* **60**, 3057–3070 (2014).
- ⁷⁹T. Lacassagne, S. Simoens, M. EL Hajem, and J.-Y. Champagne, "Turbu- 1313
lence near gas-liquid interfaces in shear-thinning dilute polymer solutions," 1314
To submit (2019).
- ⁸⁰N. T. Ouellette, H. Xu, and E. Bodenschatz, "Bulk turbulence in dilute 1315
polymer solutions," *Journal of Fluid Mechanics* **629**, 375–385 (2009).
- ⁸¹N. B. Wyatt, C. M. Gunther, and M. W. Liberatore, "Drag reduction effective- 1316
ness of dilute and entangled xanthan in turbulent pipe flow," *Journal of* 1317
Non-Newtonian Fluid Mechanics **166**, 25–31 (2011).
- ⁸²J. I. Sohn, C. A. Kim, H. J. Choi, and M. S. Jhon, "Drag-reduction effective- 1318
ness of xanthan gum in a rotating disk apparatus," *Carbohydrate Poly-* 1319
mers **45**, 61–68 (2001).
- ⁸³A. S. Pereira, R. M. Andrade, and E. J. Soares, "Drag reduction induced 1320
by flexible and rigid molecules in a turbulent flow into a rotating cylindrical 1321
double gap device: Comparison between Poly (ethylene oxide), Polyacry- 1322
lamide, and Xanthan Gum," *Journal of Non-Newtonian Fluid Mechanics* 1323
202, 72–87 (2013).
- ⁸⁴H.-W. Bewersdorff and R. P. Singh, "Rheological and drag reduction char- 1324
acteristics of xanthan gum solutions," *Rheologica Acta* **27**, 617–627 (1988).
- ⁸⁵M. Milas, W. F. Reed, and S. Printz, "Conformations and flexibility of 1325
native and re-natured xanthan in aqueous solutions," *International Journal* 1326
of Biological Macromolecules **18**, 211–221 (1996).
- ⁸⁶T. Lacassagne, S. Simoens, M. EL Hajem, and J.-Y. Champagne, "Turbu- 1327
lent dissolution and mass transfer near gas-liquid interfaces in water and 1328
shear-thinning dilute polymer solution," To submit (2019).
- ⁸⁷A. J. S. Cuthbertson, F. Samsami, and P. Dong, "Model studies for floccu- 1329
lation of sand-clay mixtures," *Coastal Engineering* **132**, 13–32 (2018).
- ⁸⁸M. Safari, M. Harris, and D. Deglon, "The effect of energy input on the 1330
flotation of a platinum ore in a pilot-scale oscillating grid flotation cell," 1331
Minerals Engineering **110**, 69–74 (2017).
- ⁸⁹W. T. Massey, M. C. Harris, and D. A. Deglon, "The effect of energy 1332
input on the flotation of quartz in an oscillating grid flotation cell," *Minerals* 1333
Engineering SI:Froth Flotation, **36-38**, 145–151 (2012).
- ⁹⁰E. A. Variano and E. A. Cowen, "A random-jet-stirred turbulence tank," 1334
Journal of Fluid Mechanics **604**, 1–32 (2008).
- ⁹¹B. Wieneke, "PIV uncertainty quantification from correlation statistics," 1335
Measurement Science and Technology **26**, 074002 (2015).